DEVELOPMENT OF ULTRA-HIGH TEMPERATURE MATERIAL CHARACTERIZATION CAPABILITIES USING DIGITAL IMAGE CORRELATION ANALYSIS

by

JULIA ELAINE CLINE

Presented to the Faculty of the Graduate School of

The University of Texas at Arlington in Partial Fulfillment

of the Requirements

for the Degree of

MASTER OF SCIENCE IN AEROSPACE ENGINEERING

THE UNIVERSITY OF TEXAS AT ARLINGTON

August 2011

To my parents, Janice and Robin Cline,

who taught me there was nothing I could not do

ACKNOWLEDGEMENTS

I wish to express my gratitude to my advisor, Dr. D. Stefan Dancila and the members of my committee, Dr. Erian Armanios and Dr. Wen Chan for their support and encouragement throughout the duration of my Masters degree. My sincerest thank you to Dr. Chan, without whom I would have not considered a graduate degree, for his advisement when I was at a crossroads in my educational career.

I had the opportunity to work with several outstanding post doctorial associates: Dr. Jennifer Goss, Dr. Xinyuan Tan and Dr. Robert Haynes. Thank you to Dr. Goss for her friendship and the special interest she has taken into my education. Thank you to Dr. Tan for her advice and encouragement over the last two years and support while TA-ing the structures lab. Thank you to Dr. Haynes for everything he has done in pursuit of our mutual research interests. I am forever indebted to him for all his hard work and guidance. I cannot hope but for the absolute best for Jenn, Yuan and Rob in their future endeavors.

My appreciation to Debi Barton, Lanie Gordon, Janet Gober, Louella Carpenter and Sally Thompson for the friendly smiles, words of encouragement, and assistance over the past few years. Even on the worst day, a visit to one of their offices always left me in a better mood. Thank you to Mike Baker for his help with any and every question I ever presented him with and for the many laughs. Thank you to Kermit Beird and Sam Williams in the machine shop for their work on machining fixtures for this project.

Thank you to Aaron Brown of Carbon-Carbon Advanced Technologies for providing me with the graphite specimens used for this work. I would like to acknowledge the authors of the software package used for this work: Christoph Eberl, Robert Thompson, Daniel Gianola and Sven Bundschuh. Thank you to Dr. Eberl for his helpful correspondence when I was first learning the program.

Finally, I wish to express my sincerest gratitude to my amazing family and friends. Words cannot begin to express my appreciation. Thank you to my cousin Chris for taking his little cousin in when she first started grad school and for his unfaltering encouragement to keep working at my degree. Thank you to my sisters, Patti and Lindsay, for their love, support and the endless stream of laughter to relieve the stress of grad school, and to Jake and Bruce for being the most loyal study companions. To my parents, Janice and Robin, thank you for teaching me that hard work does not go unrewarded. Thank you for being my inspiration, my cheerleaders, my personal financiers, and my most important teachers. I would not be who I am today, without you.

July 12, 2011

ABSTRACT

DEVELOPMENT OF ULTRA-HIGH TEMPERATURE MATERIAL CHARACTERIZATION CAPABILITIES USING DIGITAL IMAGE CORRELATION ANALYSIS

Julia Elaine Cline, M.S.

The University of Texas at Arlington, 2011

Supervising Professor: Dragos-Stefan Dancila

Ultra-high temperature deformation measurements are required to characterize the thermo-mechanical response of material systems for thermal protection systems for aerospace applications. The use of conventional surface-contacting strain measurement techniques is not practical in elevated temperature conditions. Technological advancements in digital imaging provide impetus to measure full-field displacement and determine strain fields with sub-pixel accuracy by image processing. In this work, an Instron electromechanical axial testing machine with a custom-designed high temperature gripping mechanism is used to apply quasi-static tensile loads to graphite specimens heated to 2000°F (1093˚C). Specimen heating via Joule effect is achieved and maintained with a custom-designed temperature control system. Images are captured at monotonically increasing load levels throughout the test duration using an 18 megapixel Canon EOS Rebel T2i digital camera with a modified Schneider Kreutznach telecentric lens and a combination of blue light illumination and narrow band-pass filter system. Images are processed using an open-source Matlab-based digital image correlation (DIC) code. Validation of source code is performed using Mathematica generated images with specified known displacement fields in order to gain confidence in accurate software tracking capabilities. Room temperature results are compared with extensometer readings. Ultra-high temperature strain measurements for graphite are obtained at low load levels, demonstrating the potential for

non-contacting digital image correlation techniques to accurately determine full-field strain measurements at ultra-high temperature. Recommendations are given to improve the experimental set-up to achieve displacement field measurements accurate to 1/10 pixel and strain field accuracy of less than 2%.

TABLE OF CONTENTS

LIST OF ILLUSTRATIONS

Figure Page

LIST OF TABLES

CHAPTER 1

INTRODUCTION

Thermal protection systems and heat shields are required to protect atmospheric re-entry and hypersonic flight vehicles from potentially destructive aerodynamic heating [1]. Proper understanding and characterization of material response at high temperatures is a necessary design consideration for structural components.

Accurate material characterization in an elevated temperature state introduces challenges to conventional deformation measurement techniques. Typically, deformation measurements of material specimens under load are obtained using surface-contacting methods such as electrical resistance strain gages or extensometers. Modifications to contact methods have been made to extend the application range to higher temperatures, however important limitations still exist.

Gages are highly sensitive to temperature fluctuations due to non-uniform thermal expansion of components and temperature-dependent resistivity changes. Typical gages bonded with epoxies are designed for use in the range of -103˚F to 212˚F (-75˚C to 100˚C). Higher operational temperatures have been achieved by altering bonding material. Using insulating ceramic bases, temperatures of up to 1800˚F (1000˚C) have been achieved; however the preparation is time consuming and requires skilled technique to ensure acceptable results [2].

Ultra-high temperature extensometers, for use up to 1800˚F (1000˚C) are a costly, commercially available alternative. Typically, the transducer is situated outside the furnace and long ceramic arms pass through furnace walls to contact the specimen surface. Selection is based on the heating mechanism used, and many require water-cooling during operation. An

extensometer cannot provide full-field strain measurements. Transverse strains on narrow specimens are difficult to measure because of the fixed gage length of the extensometer.

Several non-contacting optical techniques – interferometry (Moiré, holographic and speckle) and non-interferometry (automatic grids and digital image correlation) have been developed as alternatives to conventional point-wise strain measurement techniques. The advantage of optical techniques is the capability to measure full-field strain and monitor inhomogeneities without contacting the specimen surface. Interferometry methods require a complex, stability-sensitive set-up which limits the versatility of the experimental environment. Expensive coherent light sources are required to create fringe patterns from un-deformed and deformed specimens. Analysis of fringe patterns is tedious and labor-intensive despite the introduction of computational methods. Due to its comparatively simplistic, inexpensive set-up and analysis procedure, digital image correlation (DIC) has gained increased popularity as a viable strain measurement technique [3].

The digital image correlation method was pioneered at the University of South Carolina in the early 1980s and has since undergone extensive refinement. The essence is the maximization of the normalized cross-correlation coefficient, C_{xy} (Equation 1), of grayscale intensity patterns in pre-defined image subsets $(2M+1)$ x $(2M+1)$ centered around user-defined marker positions,(x_i, y_j), between images captured before and after deformation [3,4].

Using a single high-resolution digital camera fixed in a position such that the optical plane is perpendicular to the specimen, in-plane longitudinal and transverse displacement fields can be simultaneously and directly measured by marker tracking. The grayscale intensity pattern within each subset will likely be unique. Subsequent images of the deformed specimen are searched for the position,(x_i', y_j'), of the original subset that maximizes the correlation function [3-5],

$$C_{xy} = \sum_{i=-M}^{M} \sum_{j=-M}^{M} \left[\frac{f(x_i, y_j) g(x_i', y_j')}{\bar{f}\bar{g}} \right] \quad (1)$$

where, $f(x_i, y_j)$ and $g(x_i', y_j')$ are the grayscale intensity of points (x_i, y_j) and (x_i', y_j') in the undeformed and deformed images, respectively [4]. $\bar{f}$ and $\bar{g}$ are the average pixel intensity values defined as,

$$\bar{f} = \sqrt{\sum_{i=-M}^{M} \sum_{j=-M}^{M} \left[f(x_i, y_j) \right]^2} \quad (2)$$

and,

$$\bar{g} = \sqrt{\sum_{i=-M}^{M} \sum_{j=-M}^{M} \left[g(x_i', y_j') \right]^2} \quad (3)$$

Displacement vectors, **u** and **v**, for each marker can be determined by the difference between the pixel coordinates of the reference and deformed subset center points. Subsets of images are tracked, rather than individual pixels, to achieve sub-pixel resolution using interpolation-based algorithms to provide highly accurate measurements. Using equally spaced marker positions, displacements can be interpolated to provide full-field displacement measurements [3,4]. Engineering strains can be found by differentiation of the displacement field.

Specimens must have a discernable artificial or natural surface pattern to be suitable for DIC. Three criteria to define appropriate speckle patterns are generally agreed upon in literature: high-contrast, isotropic, and non-repetitive [3,4]. Unless a specimen possesses sufficient surface characteristics to satisfy these criteria, an artificial pattern must be applied to the specimen. Experimental conditions dictate how an artificial speckle pattern can be achieved. Sufficient and non-fluctuating illumination of the test specimen is often necessary for adequate contrast.

The accuracy of the method is dependent on the quality of images captured for analysis. A high-resolution digital camera, and a high-quality lens system should be used to ensure images are free from distortion [4,5].

Significant reduction or increase in strain measurements can be attributed to an induced in-plane strain field that occurs due to out-of-plane motion with respect to the camera [3,6]. Out-of-plane motion can be caused by the bending of specimens under load, Poisson's effect, and misaligned loading and gripping conditions. Displacement of the specimen away from the camera results in a shrinkage of the entire image, thereby producing apparent in-plane strain measurements that are lower than actual [3,6]. Motion toward the camera has the opposite effect, producing apparent in-plane strain measurements that are larger than actual values. Induced normal strain for a standard lens imaging a specimen experiencing out-of-plane motion, as investigated by Sutton *et al* [3,6] is linearly proportional to out-of-plane displacements, given as

$$\epsilon_{OPD} = \frac{\Delta Z}{Z} \tag{4}$$

where Z and ΔZ, are the distance between the focal point and the specimen and the out-of-plane displacement, respectively. One method to reduce this error is to increase Z. This effect can be achieved by use of a telecentric lens. Another method for eliminating out-of-plane displacement effects is the use of 3-D stereovision [3,6].

In this work, the DIC method is applied to accurately determine in-plane strains with the goal of achieving measurements of Young's modulus and Poisson's ratio for material specimens subject to thermo-mechanical loading. An innovative imaging system is developed by pairing a high-resolution digital camera and modified telecentric lens to capture highly accurate images of the specimen surface using blue-light illumination and narrow band-pass filtering.

An experimental set-up capable of achieving and maintaining temperatures up to 2000˚F (1093˚C) while simultaneously applying tensile loading and acquiring images is described and implemented. A method for applying an artificial pattern to the specimen surface capable of maintaining adhesion at 2000˚F (1093˚C) was developed to provide a high-contrasting, recognizable tracking pattern. Deformation measurements are taken using an open-source Matlab [7] based digital image correlation software [8], and the strength of the DIC method for both ambient and elevated temperature testing conditions is demonstrated.

CHAPTER 2

LITERATURE SURVEY

Thermo-mechanical material testing using DIC has been pursued to temperatures up to 2200˚F (1200˚C) [9-13]. The conventional heating mechanism is furnace-based convection/radiation methods [5,9]; however, the use of Ohmic (Joule) heating [10] and transient aerodynamic heating simulation produce faster heating times with high temperature accuracy [11,13]. Pan *et al* [13] postulate that to reach temperatures above 2200˚F (1200˚C) requires the use of a high temperature furnace or Joule heating.

Researchers have used digital image correlation techniques for measurement of thermal expansion coefficients [5, 9-13] and high temperature mechanically induced strains [9-13]. Several unique solutions have been implemented for challenging optical issues inherent in ultra-high temperature conditions that compromise the quality of DIC images.

Lyons *et al* noted that at temperatures higher than 1300˚F (700˚C) the visible radiation emitted from the specimen surface can exceed the artificial illumination incident on the specimen surface. Surface patterns became unrecognizable, and significant de-correlation occurred during DIC analysis because of increased brightness and decreased contrast [9]. Similar issues were encountered by Pan *et al* [11,13] and Grant *et al* [12]. They suggested that the combination of a brighter light source and appropriate filtering system could overcome the effects of visible radiation in the ultra-high temperature range [9-12].

It is shown that the intensity of emitted radiation in the 450 nm range is insignificant compared to light emitted in the 550 nm and 650 nm ranges [12, 13]. The use of a narrow band-pass filter centered in the blue-light range was implemented to remove the effects of radiated light in the red and green color channels from the images [12-13]. Furthermore,

supplemental illumination provided in the blue-light range is used to increase brightness to capture high contrasting images [12-13].

Optical distortion was also observed in images as a result of viewing glass imperfections [9-12] and refractive index variations due to heated gas between the specimen and the camera [9-10, 12]. Small variations in refractive index and non-uniformities within standard window glass can affect the DIC analysis. Basic translation tests were used to compare the effect of a standard furnace window glass with a high-quality optical sapphire glass [9]. An average strain of -181 με was measured for the standard glass; whereas the effect was reduced to within ±100 με using the optical glass [9]. Effects due to heated gas surrounding the specimen with varying refractive index cause localized motion in images that cannot be attributed to strain [9-12]. It is shown that the placement of a fan to disperse the heated gas would alleviate this problem [9].

Several speckle pattern techniques have been proposed using surface abrasion and scratching methods [5, 11], as conventional paints burn off at elevated temperatures [10]. Combinations of ceramic coatings [9], oxide powders, and high temperature adhesives [10,12] can be used as alternatives when surface abrasion is not possible or appropriate.

CHAPTER 3

EXPERIMENTAL APPROACH AND METHODOLOGY

Several challenges must be overcome in order to make accurate strain measurements of high temperature materials: implementation of the DIC technique by selection of appropriate software and imaging equipment, development of a temperature control system and associated gripping mechanism to simultaneously apply heating and mechanical loading, and the application of a high temperature resistant artificial surface pattern appropriate for DIC tracking.

3.1 Implementation of the Digital Image Correlation Technique

3.1.1 Digital Image Correlation using Matlab

Commercially-available digital image correlation software (VIC-2D [14], StrainMaster [15], etc) offer a user-friendly approach to image analysis. While readily available, commercial software is very costly and generally is available only as a package with the system-specific hardware. Integration with an alternate hardware set-up can be difficult because of pre-defined features within the software. Alternatively, open-source DIC codes allow the user freedom to customize existing codes for a specific application while being cost-effective (freeware) and easily accessible. *Digital Image Correlation and Tracking with Matlab* is a straight-forward, easy-to-use software developed at Johns Hopkins University by Eberl *et al* [8].

The software centers around the implementation of the Matlab [7] image registration function CPCORR, which performs normalized cross correlation of input parameters to track user-defined marker positions within un-deformed and deformed images. CPCORR can return displacement measurements up to 4 pixels with sub-pixel accuracy of 1/10 pixel. Poor

correlation will occur if marker points are defined too close to the edge of an image, within a region of low grayscale intensity variations, and if image size between the base and deformed image are different [7].

Within the CPCORR function, the variable CORRSIZE defines the region-of-interest (subset) centered on each marker point. This value can be adjusted to achieve higher spatial resolution (small CORRSIZE) or accommodate a larger pattern size (large CORRSIZE). The CORRSIZE value directly affects the marker spacing. If CORRSIZE is set to 50 pixels (100p x 100p subset centered on each marker) with a marker spacing of 100 pixels, a full-field strain measurement will be recorded. If spacing is larger than 100 pixels, gaps will exist within the strain field and data will be extrapolated to form a full-field measurement. If spacing is less than 100 pixels, adjacent markers will share pixels leading to interpolation of the displacement data [8]. Marker grids can be defined in rectangular or circular form, along a line, or as two points, depending on the tracking pattern and the desired results.

Defining a finer grid may reduce noise within the strain field, but processing time is greatly increased; conversely, a coarser grid will improve processing time but yield reduced spatial resolution. Processing time can also vary based on the CORRSIZE and the number of images processed. The preferred image format for analysis is 8-bit grayscale tagged image format (*.tif); however, faster processing can be achieved using JPEG format (Joint Photographic Experts Group) images at the cost of sub-pixel resolution [8].

Multiple images should be captured throughout the test duration to reduce the pixel displacement per image to 0.1 pixels, ideally, increasing the probability for correlation. A base image is captured prior to the start of the test to serve as a reference and define the original position of marker points for input into the correlation function. The output data from the image processing is a matrix of adjusted marker position with rows equal to the number of marker points and columns corresponding to each displaced image processed.

The post-processing component of the software provides several means of data analysis: 3-D displacement, strain measurement between 2 points, full-field strain, and 1-D strain plots; Means of removing poorly tracked markers from data sets used in strain calculations are also included. In this work, the latter two analysis methods are used. Full-field strain provides a triangle-based cubic interpolation of strain measurements for each image [8]. The 1-D strain calculation analyzes the displacement vs. position plot for each image and performs a least-squares fit (slope) of the data to calculate strain represented in that image. A strain vs. image plot is generated, of which the data can be saved for use with alternate software. The results are defined in terms of coordinate system is defined as y – direction of loading, x – transverse direction.

3.1.2 Validation: Mathematica Generated Images

In order to validate the tracking capabilities and accurately assess displacement measurements, Mathematica [16] is used to generate test images with simulated, prescribed displacements. Three 512 by 512 images of a 5 by 5 point grid are created, as shown in Figure 3.1, with specified pixel displacements based on initial position for the left column of points.

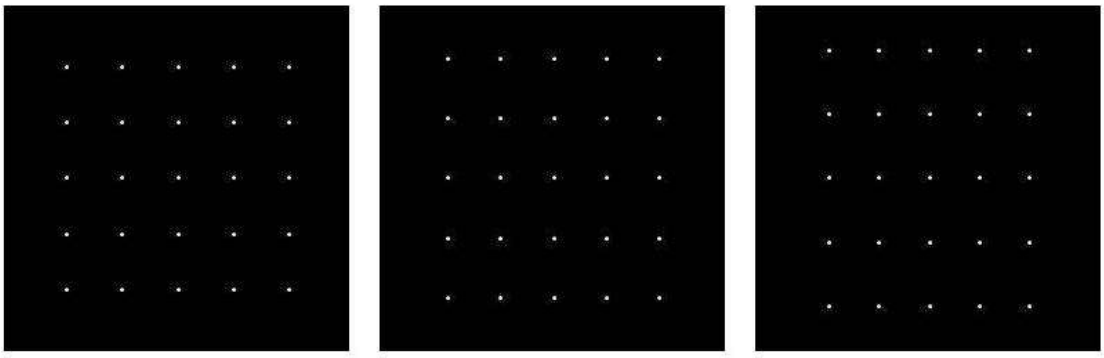

Figure 3.1 Mathematica Generated Images

The applied strain simulates rigid body translation: elongation in the longitudinal direction and contraction in the transverse direction. A grid of marker points is defined for the images and the resulting tracking data and displacements are shown in Table 3.1 and a graphical representation of the tracking pattern is given in Figure 3.2.

Table 3.1 Displaced Marker Positions and Displacement Data

Marker Position (pixels)						Displacement (pixels)			
Image 1 (grid)		Image 2		Image 3		Image 1		Image 2	
X_1	Y_1	X_2	Y_2	X_3	Y_3	ΔX_2	ΔY_2	ΔX_3	ΔY_3
177	176	181	170	185	164	4	-6	8	.12
177	216	181	213	185	210	4	-3	8	-6
177	256	181	256	185	256	4	0	8	0
177	297	181	300	185	303	4	3	8	6
177	377	181	343	185	349	4	6	8	12

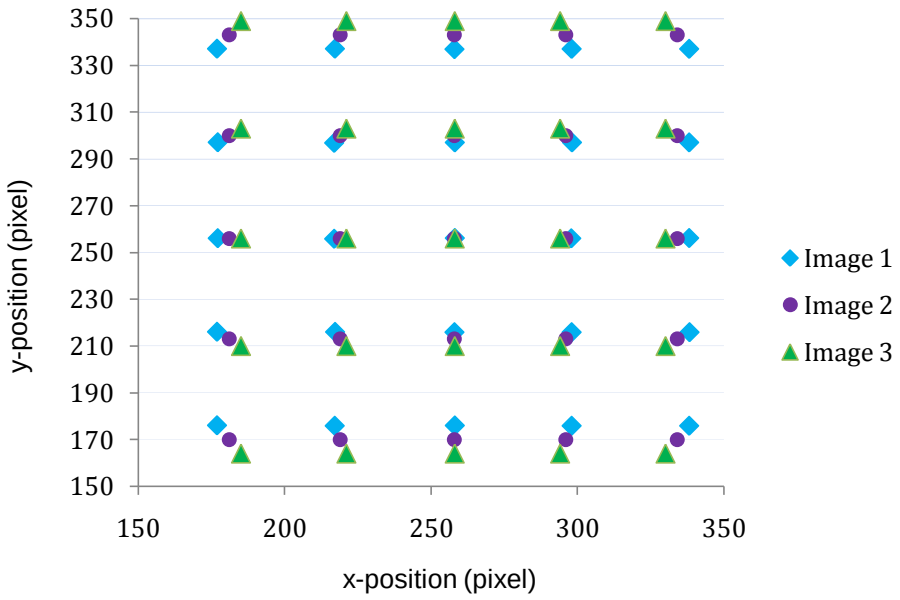

Figure 3.2 Graphical Representation of the Tracking Capabilities of Matlab Software

Tracking data exactly matched the prescribed displacement fields demonstrating the accurate tracking capabilities of the Matlab [7] software package [8].

3.1.3 Validation: Speckled Flexi-Foam Specimen

A second validation was performed on a strip of thin Flexi-foam measuring 11 in long and 4 in wide (27.94 cm by 10.16 cm) in the gage section and 1.5 in long and 4 in wide (3.81 cm by 10.16 cm) in the grip area. A high-contrasting speckle pattern, shown in Figure 3.3, was applied to the test section of the foam using a medium tipped permanent marker.

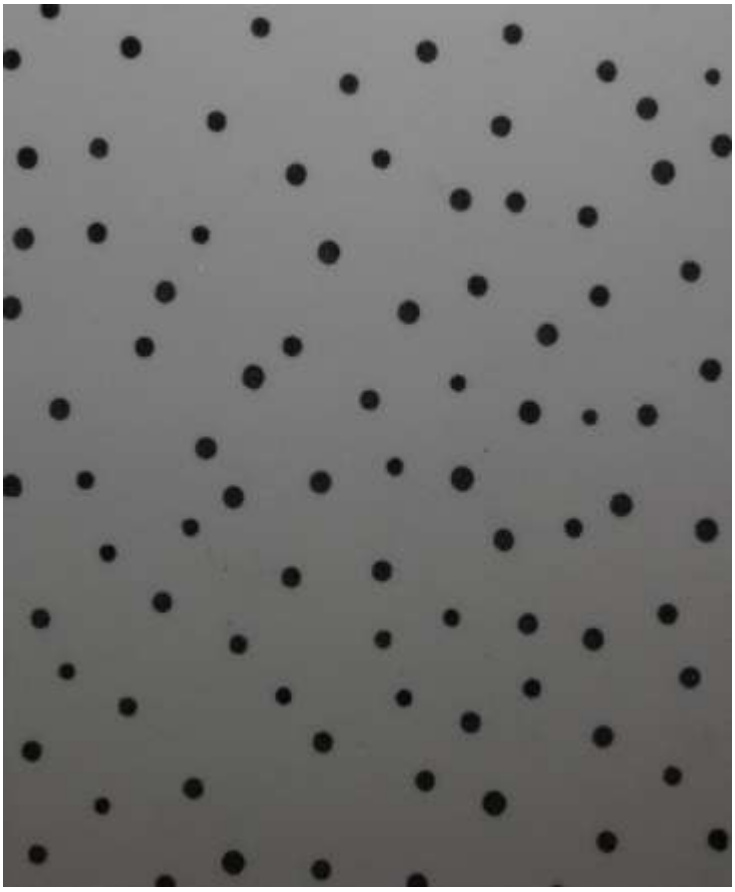

Figure 3.3 Flexi-Foam Specimen with Artificial Surface Pattern

Using a universal testing machine, described in later sections, in displacement-control mode, a displacement of 0.20 in (0.51 cm) is applied to the specimen at a rate of 0.05 in/min (0.13 cm/min). By dividing the applied crosshead displacement by the gage length, an estimation of strain in the last image is, 18182 $\mu\varepsilon$, assuming low stiffness in the specimen as compared with other components of the load train. 168 images were captured during the 4 minute test, corresponding to a capture rate of 1 image every 0.7 seconds. This ensured the pixel displacement between images was less than 4 pixels. Strain measurements as a function of longitudinal crosshead displacement in the longitudinal and transverse directions, respectively are shown in Figure 3.4 and Figure 3.5.

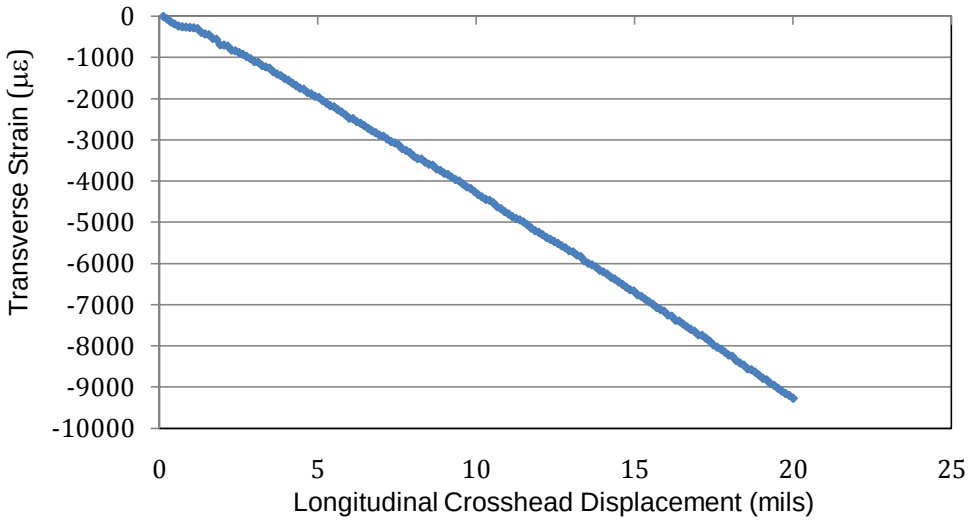

Figure 3.4 Transverse Strain Measured using DIC for Tensile Test of Flexi-Foam Specimen

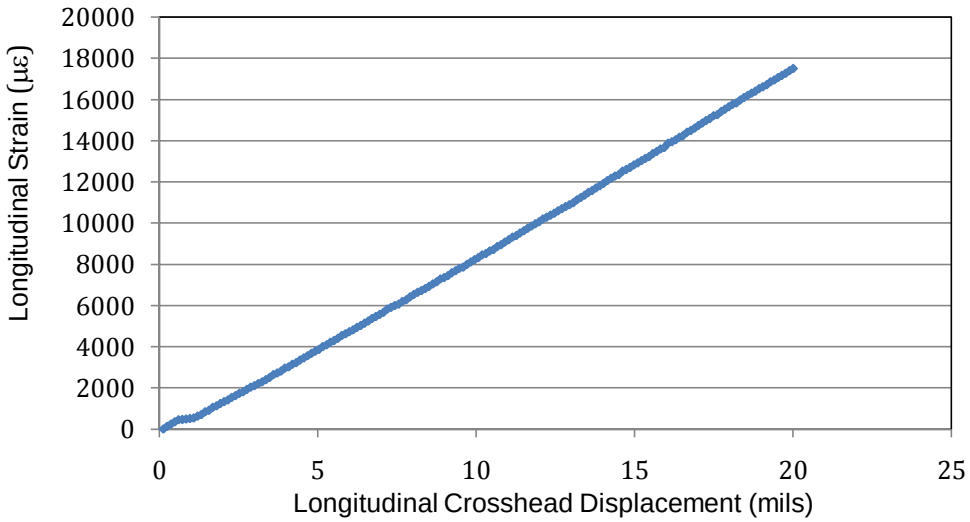

Figure 3.5 Longitudinal Strain Measured using DIC for Tensile Test of Flexi-Foam Specimen

The longitudinal strain measured at the maximum applied displacement is 17515 με, which differs from the prediction by 3.81%.

Poisson's ratio is calculated from the slope of the transverse strain vs. longitudinal strain plot shown in Figure 3.6. For this material, a value of 0.53 is calculated.

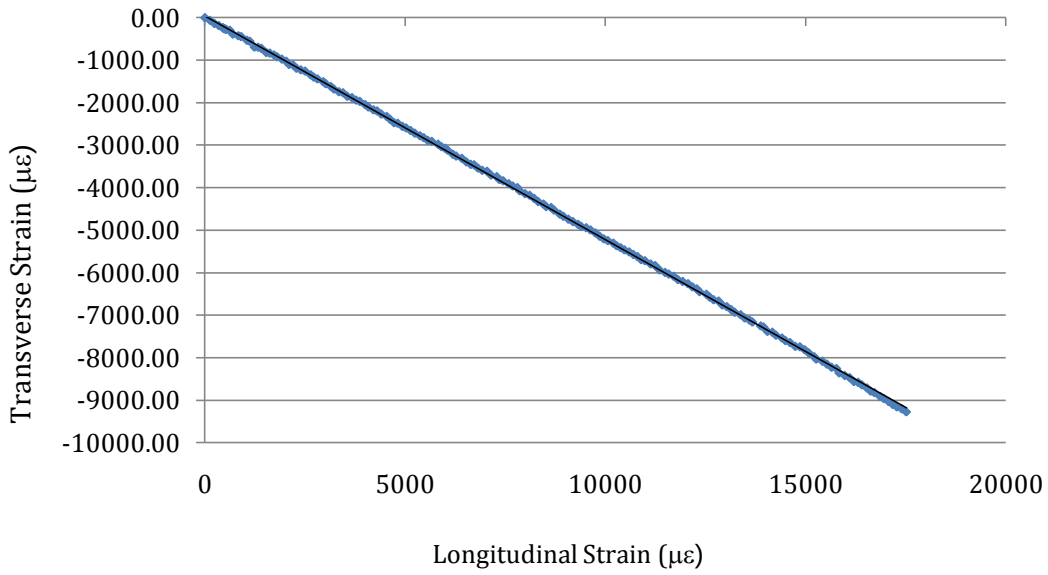

Figure 3.6 Plot of Poisson's Effect for Flexi-Foam Specimen

Results of the validation exercises confirmed that the Matlab [7] code accurately tracks deformation in the longitudinal and transverse directions respectively and returns acceptable measurements of strain per image as well as full-field strain, shown in Figures 3.7 and 3.8 for transverse and longitudinal strains, respectively.

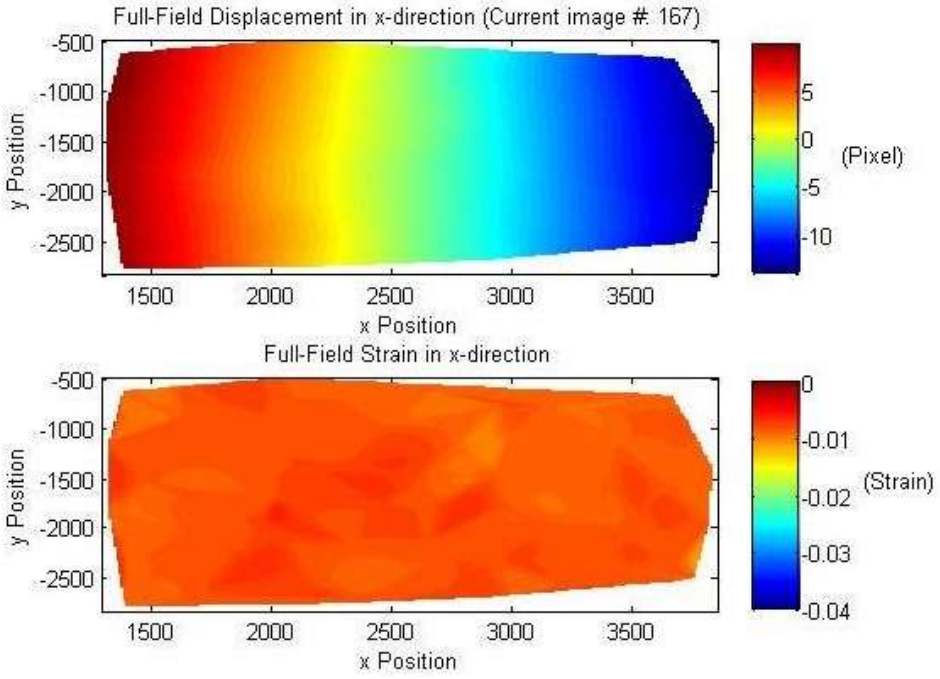

Figure 3.7 Full-field Transverse Strain for Flexi-Foam Specimen

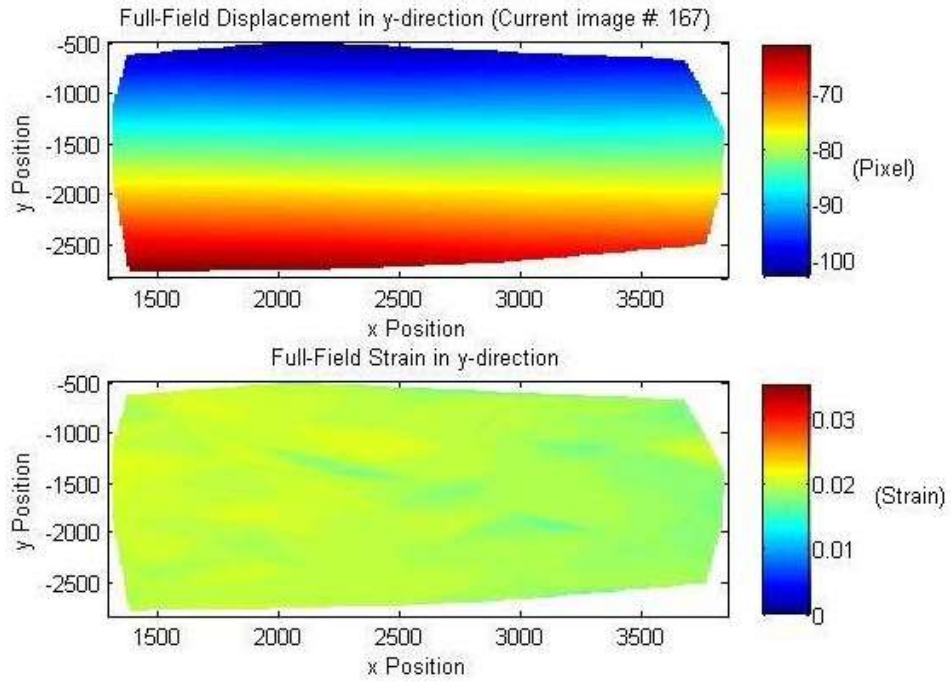

Figure 3.8 Full-Field Longitudinal Strain for Flexi-Foam Specimen

3.2 Experimental Set-up

3.2.1 Temperature Control

The temperature control system developed relies upon the electrical conductivity of the material specimens by using Joule heating to achieve desired temperatures, instead of the standard furnace-based convection/radiation heating approach. A system capable of quickly and efficiently achieving temperatures up to 2000˚F (1093˚C) is set-up using a digital PID controller, C-type thermocouple, solid state relay (SSR), and a 225 A/25V step-down voltage transformer. Temperature sensing capabilities of the system are limited by 1) thermocouple type and maximum temperature and 2) maximum amperage of the transformer. A schematic diagram is shown in Figure 3.9.

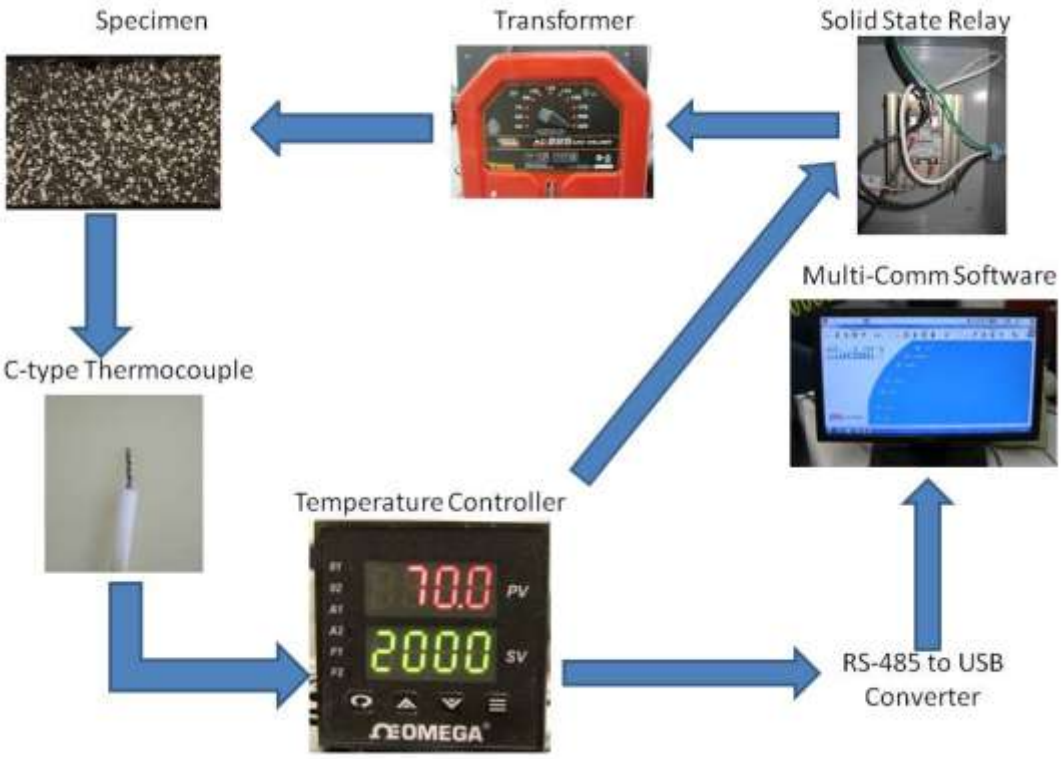

Figure 3.9 Schematic Diagram of Temperature Control System

An Omega CN8201-DC1 C4 proportional-integral-derivative (PID) digital temperature controller with RS 485 communication is connected to a computer using an RS 485 to USB converter cable and operated using Athena Multi-Comm version 3.16 software [17]. The auto-tune feature establishes PID gains prior to reaching the set point, ensuring fast response and overshoot. The auto tune feature was used the first time the system was run. An initial overshoot of 0.4% is observed at 2000˚F (1093˚C), but stabilizes within approximately 10 seconds and maintains the temperature within 0.15% of 2000˚F (1093˚C) for the duration of the test. A sample temperature profile is shown in Figure 3.10. To heat to another temperature value, the set-point is adjusted and the system adjusts its parameters accordingly.

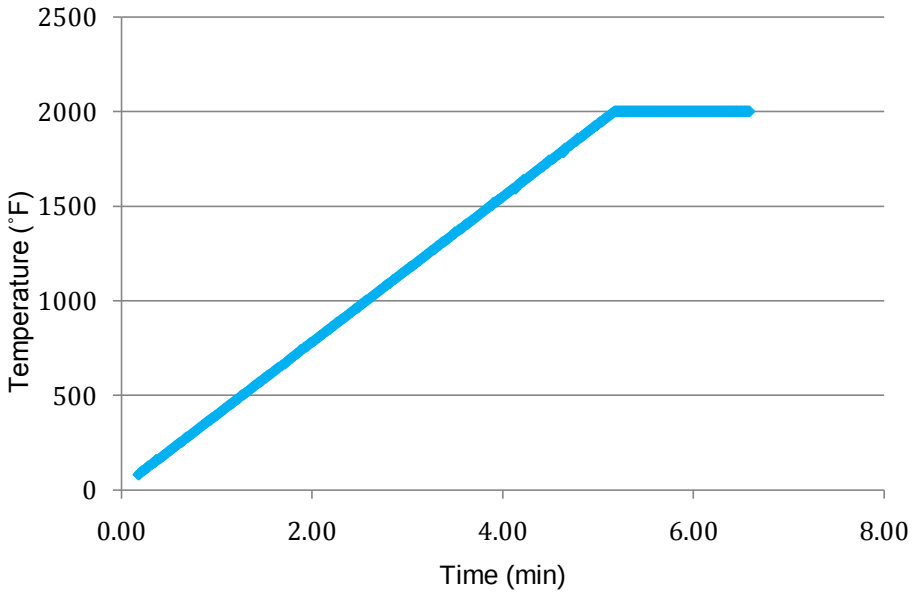

Figure 3.10 Temperature Profile of 5 Minute Ramp to 2000˚F

A 0.50 mm (0.02 in) diameter C-type thermocouple (Tungsten 5% Rhenium – Tungsten 26% Rhenium) with a maximum temperature of 4199˚F contacts the specimen surface and provides input to the temperature controller. An alumina sheathing with a maximum service

temperature of 3450˚F electrically insulates the thermocouple during testing. Corresponding C-type connectors and extension wire attach the thermocouple to the temperature controller input.

A solid state relay (SSR) with on/off functionality controls electrical power from an alternating current supply, which powers a Lincoln Electric AC 225A Arc Welder step-down voltage transformer. A 5V control signal is sent from the controller to the SSR to switch the transformer on-and-off, adjusting the current flowing through the specimen, which in turn controls the specimen temperature. The SSR is mounted to a finned heat sink to dissipate the heat generated by the voltage drop across the switch. The current output range for the transformer is 40 to 225 A in 15 to 25 A increments with a maximum allowable 20% duty cycle at 225 A.

The current settings required to heat a specimen to a desired temperature must be determined for each new material system. The internal resistance of the specimen is measured using a digital multi-meter and an initial estimate for required current is calculated based on voltage output of 25 volts. A test of the temperature control system is then performed using this amperage to ensure the desired temperature can be achieved in a reasonable amount of time.

The electrodes from the arc welder are removed and cable lugs are attached to the cable ends. The electrical cables are then attached to the high-temperature grips to apply current to the specimen which is described in a later section.

The material specimen is insulated by a double walled enclosure, shown in Figure 3.11, made of 0.5 in thick alumina board to contain the radiated heat. A 1.50 in (3.81 cm) diameter circular cut-out on the front face allows illumination of surface and image capture of the gage section. Small inlets, 0.13 in (0.32 cm) diameter, on the backside of the enclosure are made for insertion of the thermocouple and Argon gas.

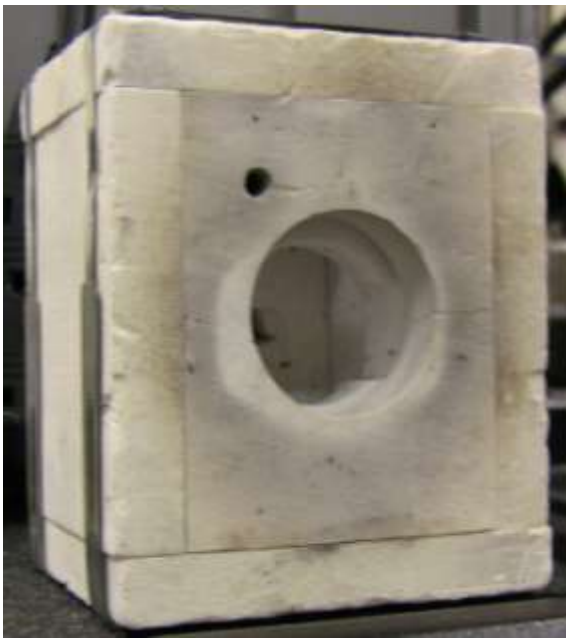

Figure 3.11 Alumina Insulating Enclosure with Circular Viewing Window

3.2.2 Oxidation Prevention

To prevent oxidation of the specimen surface, tests must be performed in an oxygen-free, inert atmosphere [18]. A sealed enclosure, shown in Figure 3.12, 26 in tall by 12 in wide by 8 in deep (40.64 cm by 30.48 cm by 20.32 cm) was manufactured to contain the inert atmosphere. A clear glass viewing window provides a view to the specimen, and inlets were made for the thermocouple, electrical cables, and gas flow. Argon was selected as the inert environment because of its non-reactive properties.

Figure 3.12 Sealed Argon Enclosure

Since argon is denser than oxygen, argon enters the enclosure through an inlet at the base and oxygen is flushed out at the top. A secondary flow of argon is directed into the insulating alumina enclosure to ensure the air surrounding the specimen and thermocouple is oxygen-free. The entire system is flushed for 5 minutes prior to testing at a rate of 1.5 cubic feet per minute (0.04 m^3/min). Gas flow is maintained throughout the test duration and afterward, until the specimen cools to a temperature below the oxidation range.

Dimensional measurements taken for each material specimen before and after testing showed a minimal reduction in width and thickness of less than 1 %.

3.2.3 Load Application

The operating temperature for this work far exceeds the range of any commercially available gripping mechanism. A combination of Instron wedge grips and custom-designed high-temperature grips is used to simultaneously apply Joule heating and monotonic loading.

As seen in Figure 3.13, a 2 in by 2 in (5.08 cm by 5.08 cm) glass epoxy panel is loading into the Instron wedge grips to provide electrical insulation to the heating system.

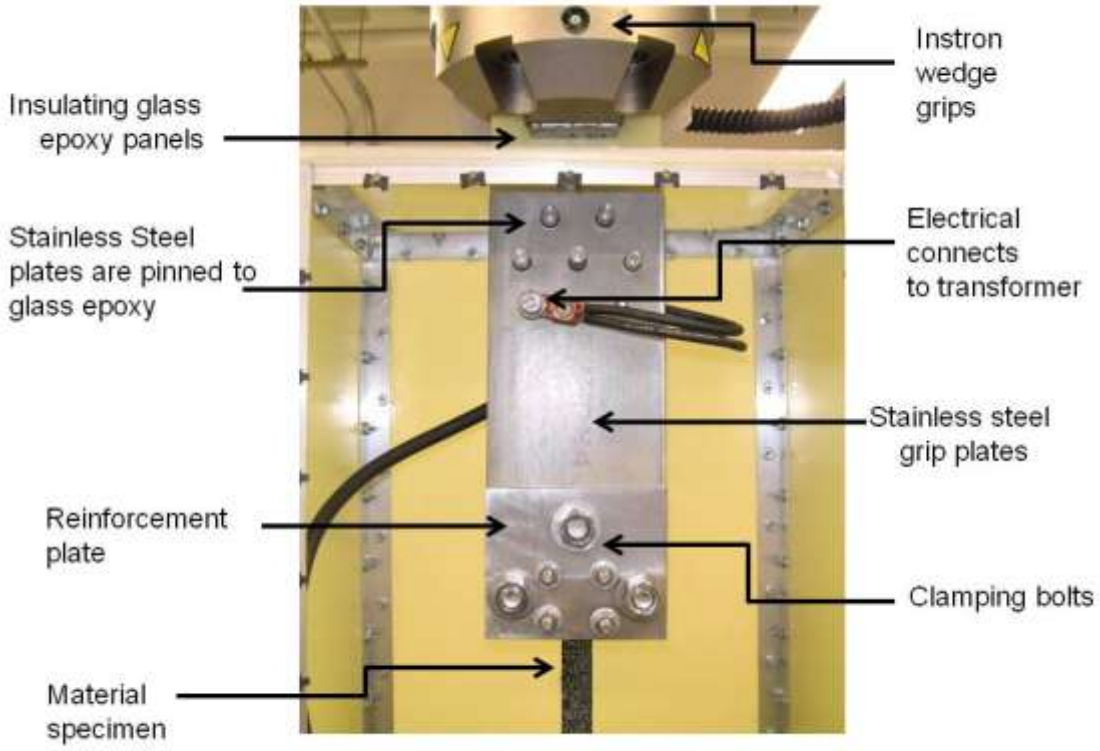

Figure 3.13 High Temperature Gripping Mechanism Diagram

Two stainless steel plates with horizontal jaw faces are pinned to the glass epoxy panel at the top (shown in Fig 3.13). A material specimen is clamped between the two plates which are bolted together to a specific torque level such that the specimen will not slip during loading. The

electrical cables from the transformer are attached to either side of the grips which apply a closed-loop, even distribution of electrical current. This set-up is mirrored for the bottom grip.

The grips are installed into an Instron 5885 electro-mechanical axial testing machine which is operated using Windows-based Bluehill [19] software. Tensile test methods are written within the software to apply monotonically increasing loads at rates of 0.01 in/min (.03 cm/min) at room temperature and 0.02 in/min (0.05 cm/min) at high temperature, to account for thermal expansion. For room temperature testing, an Instron 1-in extensometer is attached to measure longitudinal strain (Fig. 3.14). A digital output signal from the controller is used to trigger image capture at 20-lb (89 N) increments.

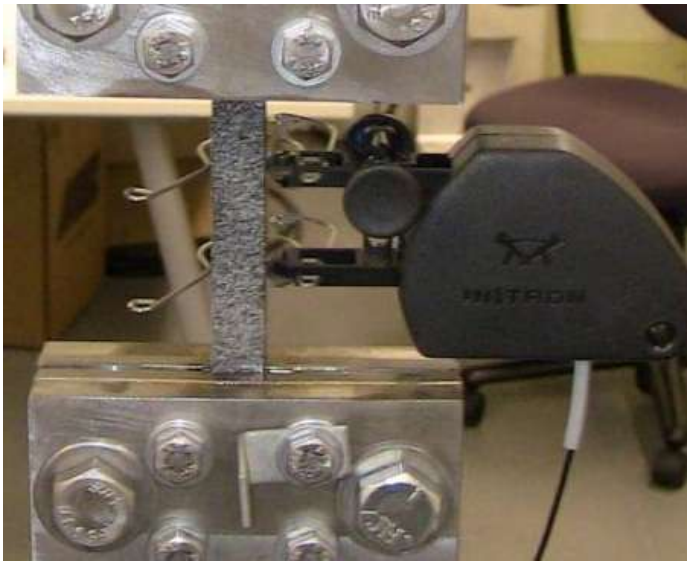

Figure 3.14 Longitudinal Extensometer Attached for Room Temperature Tests

3.2.4 Image Capture System

As stated previously digital image correlation requires accurate images of the specimen surface [3,4]. Any sources of optical distortion must be removed or reduced to an negligible amount to reduce de-correlation during image processing.

3.2.4.1 Camera and Mount

The camera selected for this work is an 18 megapixel Canon EOS Rebel T2i with a 1.2 in (30.48mm) class CMOS sensor. Shutter speed and ISO settings can be manually set and range from 10 to 1/4000 seconds and 100 – 6400, respectively. Each image is comprised of 5184 pixels by 3456 pixels which correspond to an imaging area of 1.10 in by 0.73 in (2.79 cm by 1.85 cm).

The camera is mounted to a low friction travelling stage to allow simple focal adjustments and is placed on a level platform that ensures it is perpendicular to and in-line with the center of the specimen. The travelling stage is attached to the high temperature grips by way of an insulating glass epoxy arm, as shown in Figure 3.15 that ensures the camera remains a fixed distance from the specimen even in the event that out-of-plane displacement is greater than the telecentric depth.

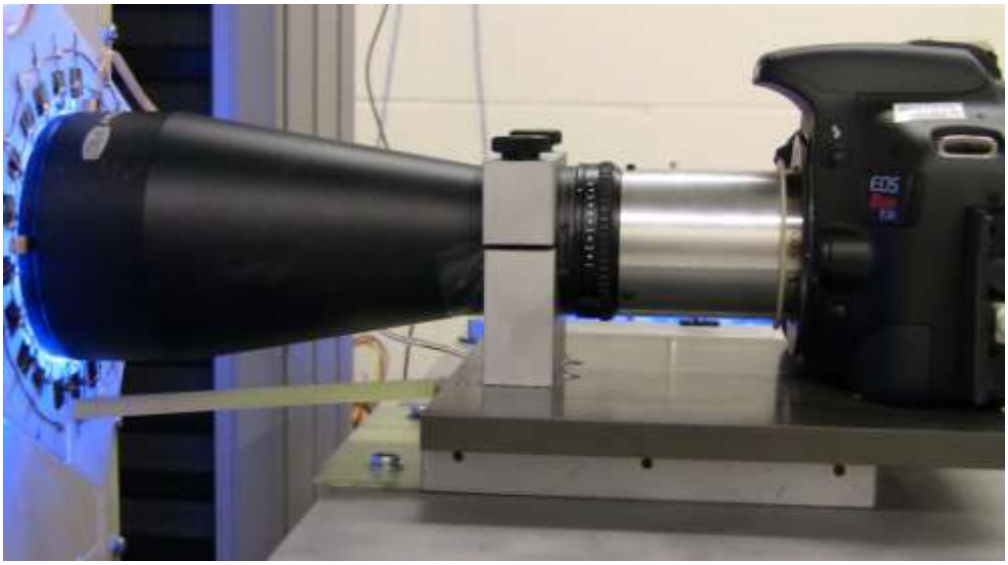

Figure 3.15 Camera Mount Connection to High Temperature Grips

3.2.4.2 Telecentric Lens

An object-sided telecentric lens is used to increase the effective distance to the specimen by placing the entrance pupil at infinity and thereby reducing out-of-plane motion to effects within the images. This ensures that the principal light ray travels parallel to the optical axis, shown in Figure 3.16 [20]. Images are captured at constant magnification, thereby preserving dimensions and are insensitive to small changes in distance between the object and the camera [20].

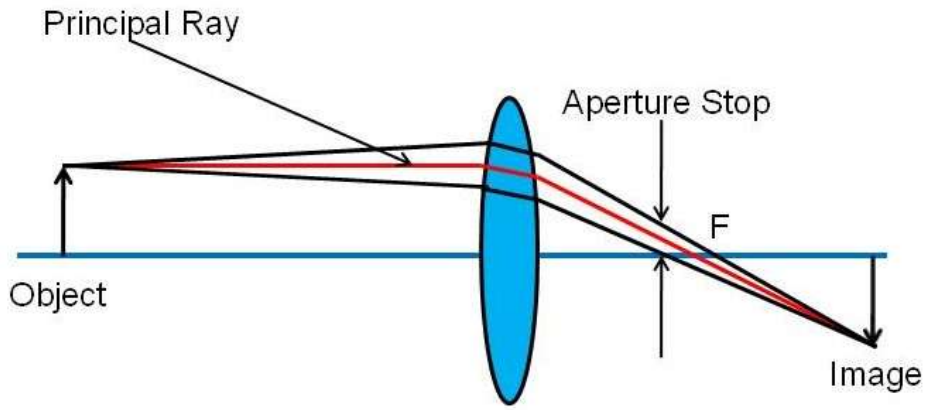

Figure 3.16 Focal Diagram for an Object-Sided Telecentric Lens [20]

Typically, telecentric lenses are designed for certain camera mounts. A Canon EF-mount is designed to work at 1.73 in (43.94 mm). A C-Mount Schneider Kreutznach (0.79x) telecentric lens with a flange focal distance of 0.68 in (17.52 mm) was modified to work with the Canon EF- mount by shortening the lens tube. The optics of the telecentric lens were not affected. In this way, the Canon digital camera and telecentric lens can be combined to achieve a high resolution imaging system. The working distance of the lens is 4.17 in (106mm) with a telecentric depth of 0.08 in (2.03 mm). The telecentric range of this camera system is verified by translation tests using a micrometer and compared with an identical test using a standard macro lens. A specimen is placed at the correct working distance of the camera and translated toward and away from the camera at 0.004 in (0.10 mm) intervals to ± 0.08 in (2.03 mm). The images are processed with the digital image correlation software and the apparent strain fields in the images are generated. Figure 3.17 shows a comparison of the induced strain fields for the telecentric and macro lenses.

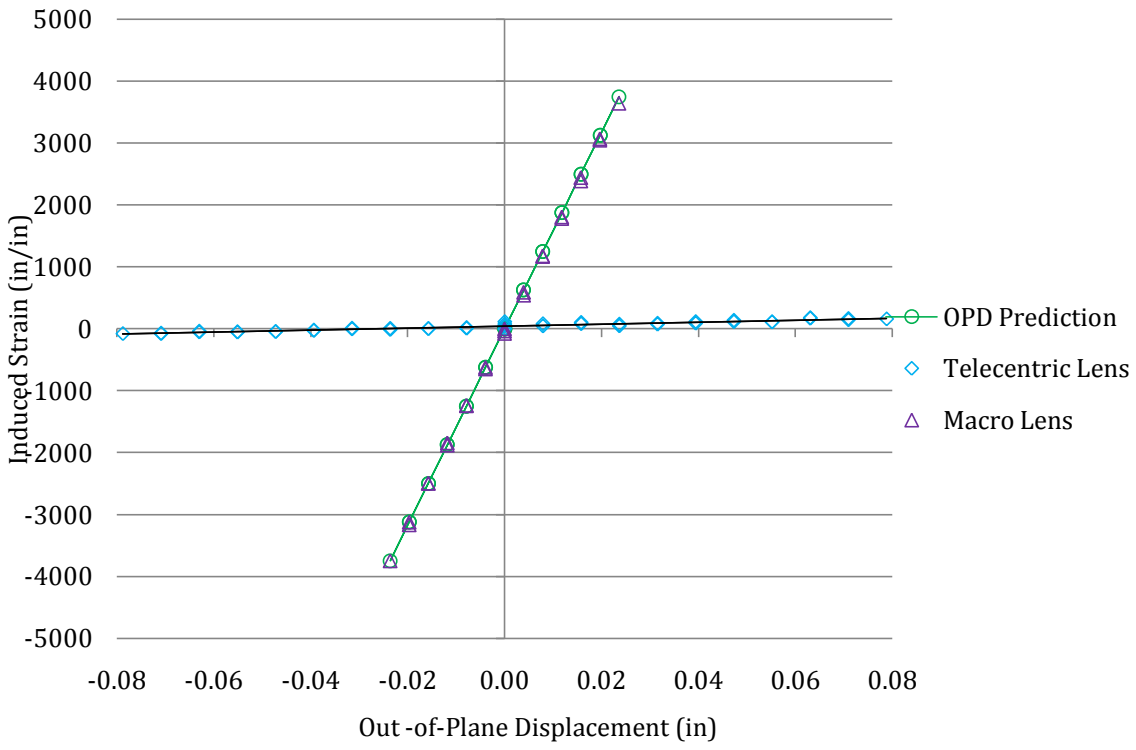

Figure 3.17 Comparison of the Induced In-Plane Strain Field caused by Out-of-Plane Displacement in a Macro Lens and Telecentric Lens

An in-plane strain field of 15693 με / in (6157.4 με / mm) of out-of-plane displacement can be expected for images captured using a macro lens. The induced in-plane strain field for the macro lens is accurately predicted using equation 4 from Chapter 1 for a specimen placed 6.3 in (160.02 mm) from the camera

It is verified that the use of a telecentric lens effectively reduces the effects of out-of-plane displacement to 1613.1 με/in (63.6 με /mm), nearly 10 times less than the macro lens. The use of this lens, combined with restricting out-of-plane motion within the experimental set-up to less than 0.01 in, results in a introduced strain field of 16.13με, which is negligible.

3.2.4.3 Illumination and Camera Filters

Specimens should have sufficient illumination by either natural or artificial-light sources throughout the duration of the test [3,4]. Brightness and contrast differences between images due to insufficient lighting can introduce non-deformation related intensity shifts to experimental data and should be avoided.

The use of camera filters can reduce the amount of light incident on the camera's sensor to allow the camera to extend the range of the camera to be used in brighter settings, which is particularly useful for imaging high-temperature surfaces. The appropriate combination of illumination and camera filters is imperative to capture high-quality images.

A B&W F-Pro UV-IR-Cut multi resistant coating (MRC) filter blocks out ultraviolet and infrared radiation which causes optical distortion due to chromatic aberration. The pass wavelength range is 390 to 690 ± 15 nm. It provides added protection to the imaging and lighting system to prevent overheating.

A hot mirror is an economical alternative to a UV-IR-Cut filter when the primary concern is blocking infrared radiation rather than ultraviolet. Hot mirrors can be purchased in a select range of sizes, mounted and un-mounted and could be considered as a replacement for the imaging window of the high-temperature enclosure to reduce optical distortion and prevent glass cracking due to thermal effects.

At room temperature, two EcoSmart Par 38 18 Watt (75 Watt equivalent) light-emitting diode (LED) flood lamps are placed on either side of the camera, angled toward the specimen. The intensity of the reflected light from the specimen can overwhelm the camera sensor resulting in overexposed images, so a Tiffen ND0.9 Neutral Density filter is used to reduce the incident light by 90%. Using this method, images captured at a 1/20 shutter speed and ISO of 200 have a high-contrast pattern with minimal lighting effects.

Initially, image capture at high-temperature was performed using the neutral density and UV-IR-Cut filters and radiated light from the specimen. The features of the speckle pattern

did not appear as crisp at high-temperature as compared to room temperature as shown in Figure 3.18.

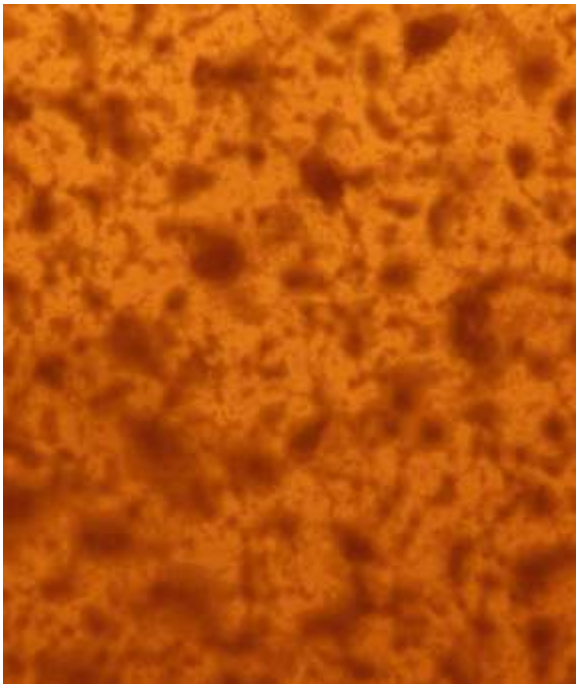

Figure 3.18 Specimen Surface at 2000°F (1093˚C) using Radiated Light viewed through Neutral Density Filter (SS. 1/20; ISO 200)

This is possibly due to a gradient in the opacity of each speckle, where the thinner outer edges allow the passage of some light. The lack of sharpness leads to poor tracking in the DIC software and subsequently, inaccurate strain measurements. Similar issues were observed by Pan *et al* [13] and Grant *et al* [12], leading to the development of the blue-light illumination and narrow band-pass filter method for capturing ultra-high temperature images derived from black body radiation.

Any heated object emits electromagnetic radiation with peak intensity proportional to wavelength and temperature as described by Planck's law,

$$I(\lambda, T) = \frac{2hc^2}{\lambda^5} \frac{1}{e^{hc/\lambda kT} - 1} \quad (5)$$

where,

I = Intensity of Radiated Light, W m^{-2}

λ =Wavelength, nm

h = 6.626068 x 10^{-34} m^2 kg s^{-1}, *Planck's Constant*

c = 2.99792 x 10^5 km/s, *speed of light in vacuo*

k = 1.3806503 x 10^{-23} m^2 kg s^{-2} K^{-1}, *Boltzmann Constant*

As temperature increases the peak wavelengths shortens, and overall brightness of images increases drastically. The intensity of radiated light in the peak red (650 nm), green (550 nm) and blue (450 nm) wavelengths is shown in Figures 3.19, 3.20 and 3.21 respectively. The radiation energy dissipated by at each wavelength is summarized in Table 3.2.

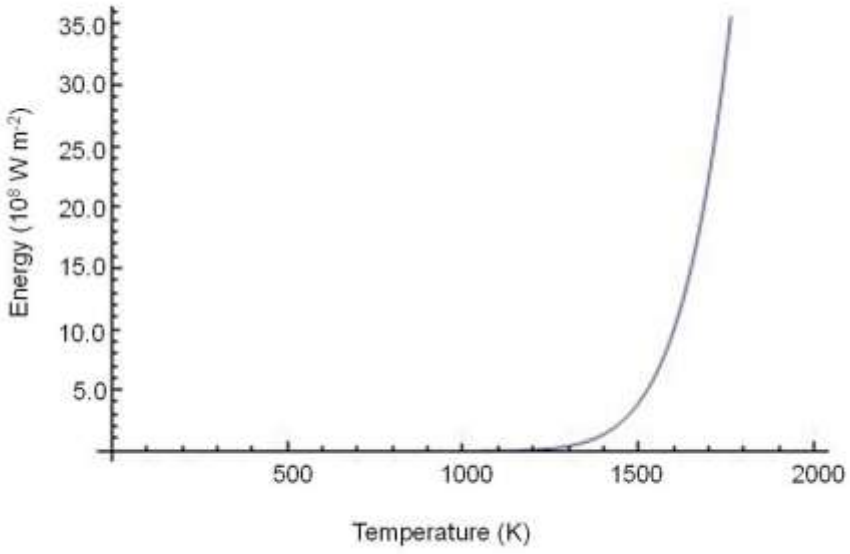

Figure 3.19 Intensity of Radiated Light as a Function of Temperature in the Peak Red Wavelength (650 nm)

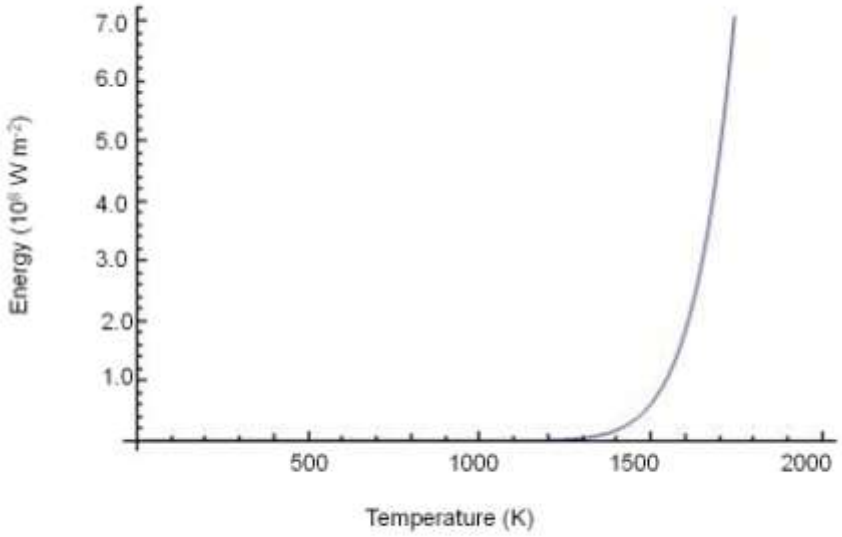

Figure 3.20 Intensity of Radiated Light as a Function of Temperature in the Peak Green Wavelength (550 nm)

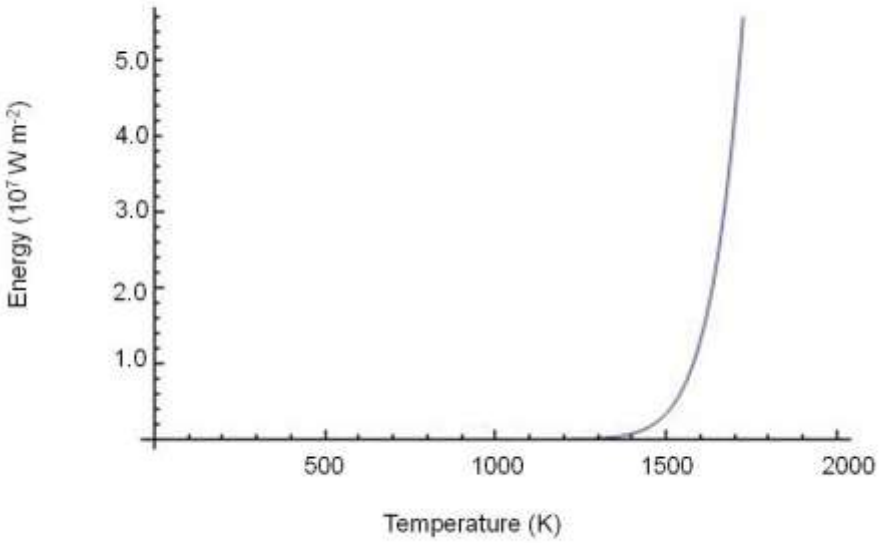

Figure 3.21 Intensity of Radiated Light as a Function of Temperature in the Peak Blue Wavelength (450 nm)

Table 3.2 Radiation Energy for Red, Green and Blue Wavelengths at 2000˚F (1093˚C)

Wavelength (nm)	Energy (W m^{-2})
650 (Red)	1.5844×10^{10}
550 (Green)	4.87175×10^{9}
450 (Blue)	7.23855×10^{8}

A ring light comprised of 20 ultra-high brightness 0.4 in (10 mm) blue LED lights is mounted to the camera lens system shown in Figure 3.22.

Figure 3.22 Blue-light Illumination

Each LED outputs 8000 mcd (milli-candelas) of light with wavelengths between 465 nm to 467.5 nm over a viewing angle of 16˚. This lighting combined with a blue band pass filter with a

transmission range of 465 nm ± 25 nm effectively eliminates the effect of radiated light in the images, as shown in Figure 3.23.

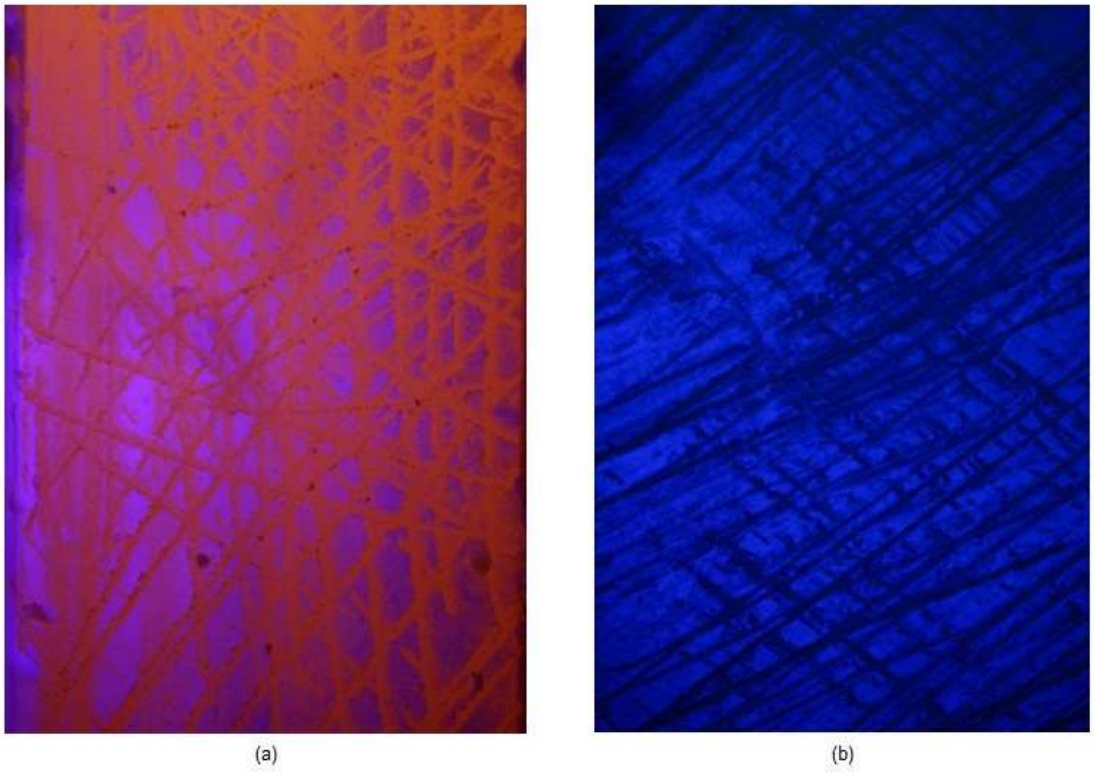

Figure 3.23 Comparison of images captured with blue-light illumination (a) without and (b) with blue band pass filter

Figure 3.23 (b) is an example of a raw image captured during testing. The Mathematica [16] image processing and analysis tool ColorSeparate is used to isolate the blue color channel image from RGB images. As shown in Figure 3.24, the red and green color channels are nearly black, indicating that any effect of radiated light is removed from the images using the band pass filter. The blue channel, due to proper illumination, contains an image with appropriate contrast and pattern for digital image correlation.

Figure 3.24 (a) Red, (b) Green, and (c) Blue color channels for Figure 3.23 (b)

3.2.5 Specimen Preparation

Carbone 2020 (graphite) is machined into 8.00 in (20.32 cm) long dog-bone specimens with a 2.24 in long by 0.50 in wide gage section (5.69 cm by 1.27 cm); 2.00 in long x 1.00 in wide gripping area (5.08 cm by 2.54 cm); and a thickness of 0.20 in (0.51 cm).

The specimen surface is cleaned using 91% isopropyl alcohol and acetone prior to pattern application. A sufficient, ultra-high temperature resistant, high-contrast pattern can be created using Sauereisen Aluseal 2, ultra-high temperature sodium-silicate adhesive cement. Several specimens are speckled using a small paint roller to spread a thin layer of adhesive in a random pattern on the specimen surface. It was observed in several preliminary tests that though adequate pressure is applied to promote adhesion to the specimen surface, this pattern application technique did not hold at 2000˚F (1093˚C).

It was found that if a thin layer (0.001 – 0.002 in; 0.003 – 0.005 cm) is spread on the specimen surface and scraped away to a very thin layer and a stick pin is used to create a scratch pattern that the adhesion to the specimen surface was much more effective. The adhesive is left to cure for 24 hours at room temperature prior to testing.

3.3 Experimental Procedures

For the graphite specimens, the current required to heat the specimens to 2000˚F (1093˚C) is 225 A. The heating cycle is set to a 5 minute ramp, taking into account the duty cycle of the transformer. Argon flushing is commenced 5 minutes prior to the start of the test.

The camera is focused using the EOS Utility [21] accompanying software. Coarse focal adjustment is done first and then using a zoomed live-shoot view, fine focal adjustment is performed to ensure crisp definition within the images.

Table 3.3 Camera settings for Room and High Temperature tests

	ISO Setting	Shutter speed (s)
Room Temp. (70˚F)	200	1/20
Ultra-High Temp. (2000˚F)	200	1/100

The ISO value is purposely kept low to ensure the camera sensor is less sensitive to the light generating images with a finer grain and thus, increased sharpness.

For high temperature tests, it is recommended, if possible, to apply a pre-load to the specimen prior to heating to account for thermal expansion. It is very difficult to apply a pre-load to the graphite specimens due to their brittle response and low strength, so the load is very carefully monitored and adjusted during the heating cycle to ensure that the specimen does not prematurely fracture.

Once the desired temperature level is achieved a base image is recorded and the trigger switch is locked in place. This allows the digital output from the controller to automatically trigger the camera at specified intervals. The test method in the Bluehill [19] software is started immediately after the base image is taken.

CHAPTER 4

RESULTS AND DISCUSSION

4.1 Room Temperature Tensile Tests using DIC

Tensile tests are performed on graphite specimens at room temperature and strain is measured using a longitudinal extensometer in addition to digital image correlation to verify the accuracy of the DIC measurements. Comparison data for percent difference between extensometer and digital image correlation measurements are presented.

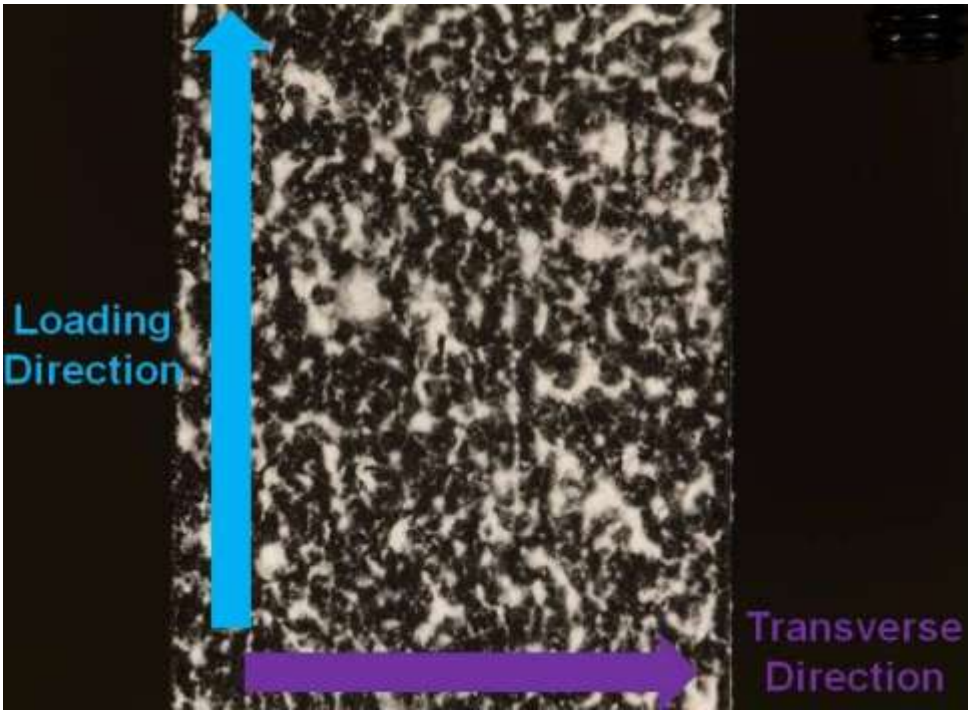

Figure 4.1 Sample Room Temperature Image (SS.1/20; ISO 200)

Images, as seen in Figure 4.1, are processed with a CORRSIZE of 100 and marker spacing in each direction of 200 in order to cover the full strain field.

The strain per stress level graphs for the longitudinal (loading) and transverse directions are obtained from DIC analyses and are shown in Figure 4.2 and Figure 4.3, respectively.

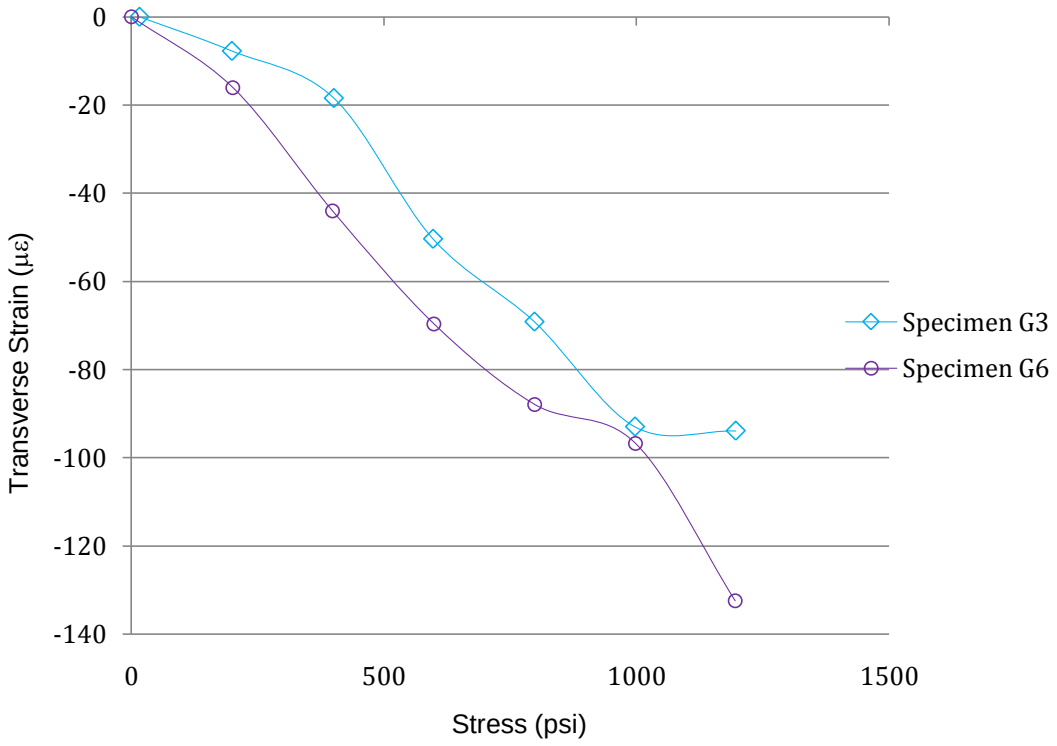

Figure 4.2 Transverse Strains per Stress Level for Specimens G3 and G6

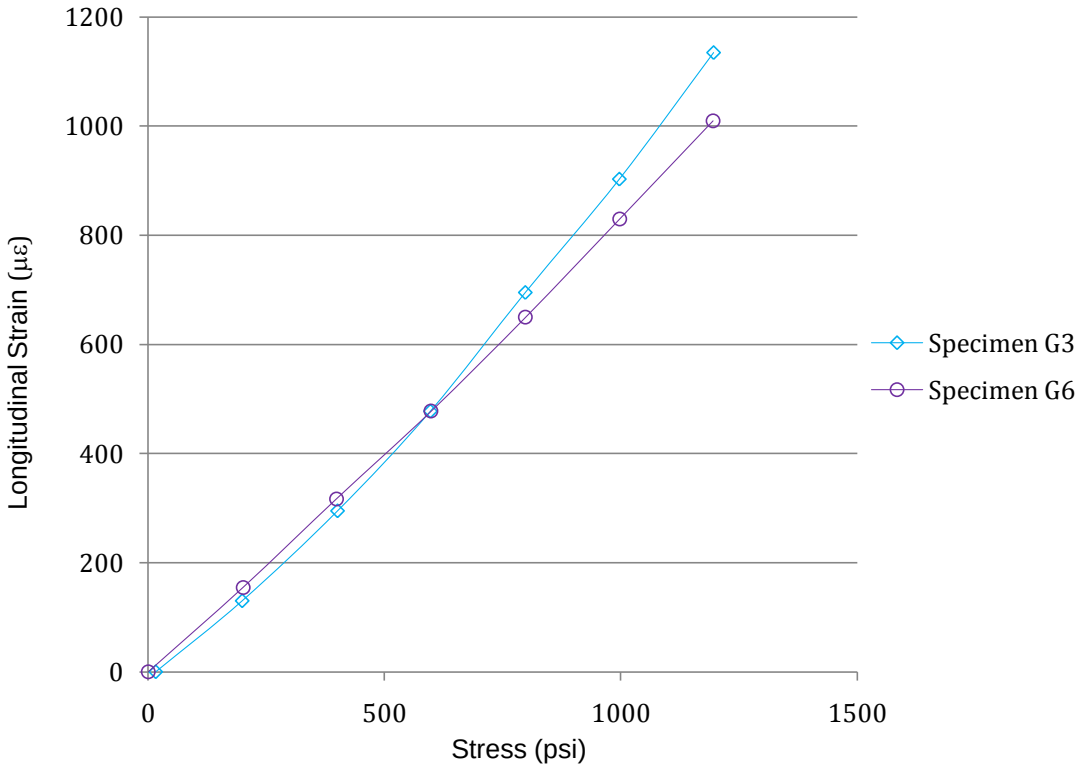

Figure 4.3 Longitudinal Strains per Stress Level for Specimens G3 and G6

Comparison of strain measurements between extensometer and DIC is shown in Table 4.1 for room temperature tests.

Table 4.1 Strain Measurements from Extensometer and DIC for Specimen G3

Image number	Load (lbf)	Extensometer Strain (με)	DIC Strain (με)	Percent Difference (%)	Stress (psi)
1	1.60	-50.00	0.00	-	15.94
2	19.96	110.00	130.07	18.24%	198.81
3	40.21	300.00	294.89	-1.70%	400.59
4	59.93	490.00	477.59	-2.53%	597.78
5	80.08	700.00	695.04	-0.71%	797.78
6	100.05	920.00	902.78	-1.87%	996.77
7	120.06	1150.00	1134.60	-1.34%	1196.14

Table 4.2 Strain Measurements from Extensometer and DIC for Specimen G6

Image number	Load (lbf)	Extensometer Strain (με)	DIC Strain (με)	Percent Difference (%)	Stress (psi)
1	0.02	-70.00	0.00	-	0.21
2	20.16	110.00	154.84	40.76%	200.87
3	39.97	290.00	316.85	9.26%	398.24
4	60.12	460.00	477.74	3.86%	598.91
5	80.14	640.00	649.63	1.50%	798.39
6	100.16	820.00	830.10	1.23%	997.84
7	119.97	1010.00	1009.93	-0.01%	1195.24

At low strain levels, the percent error of the DIC measurements is significantly higher than desired. This is because the method is unable to resolve very low strain levels [3]. As shown in Figure 4.4, correlation in measurements is achieved at higher strain levels where error is reduced to less than 2%. For this reason, data points at low strain levels are omitted from calculations of material properties to ensure accurate results.

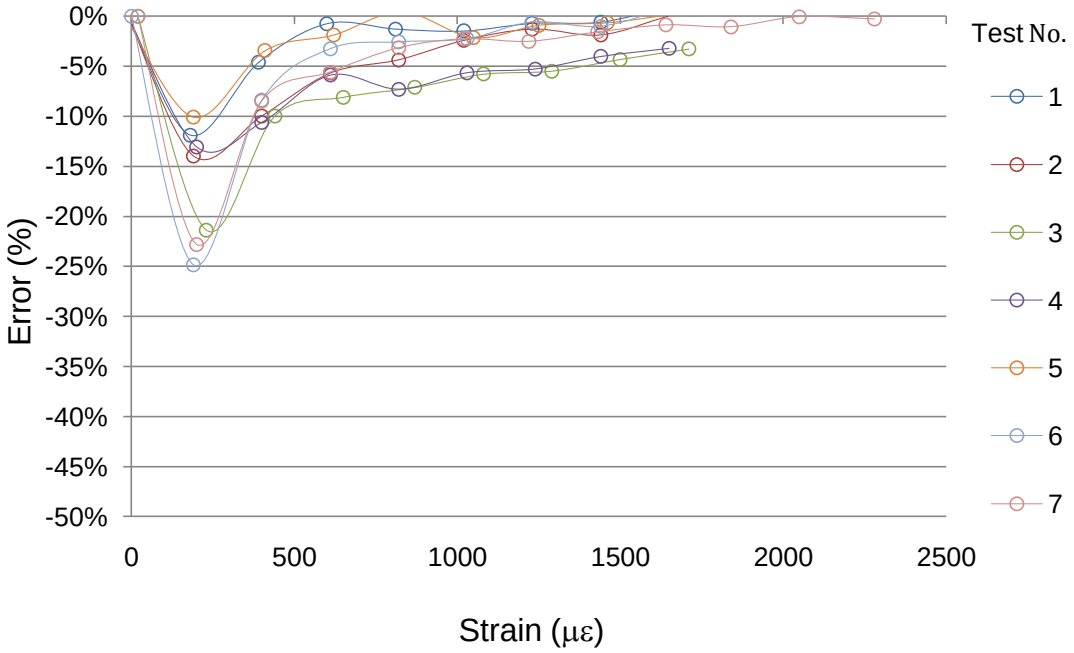

Figure 4.4 Percent Error in DIC Strain Measurements per Strain Level

Figure 4.5 shows the stress vs. longitudinal strain plot for two room temperature tests with extensometer and DIC measurements.

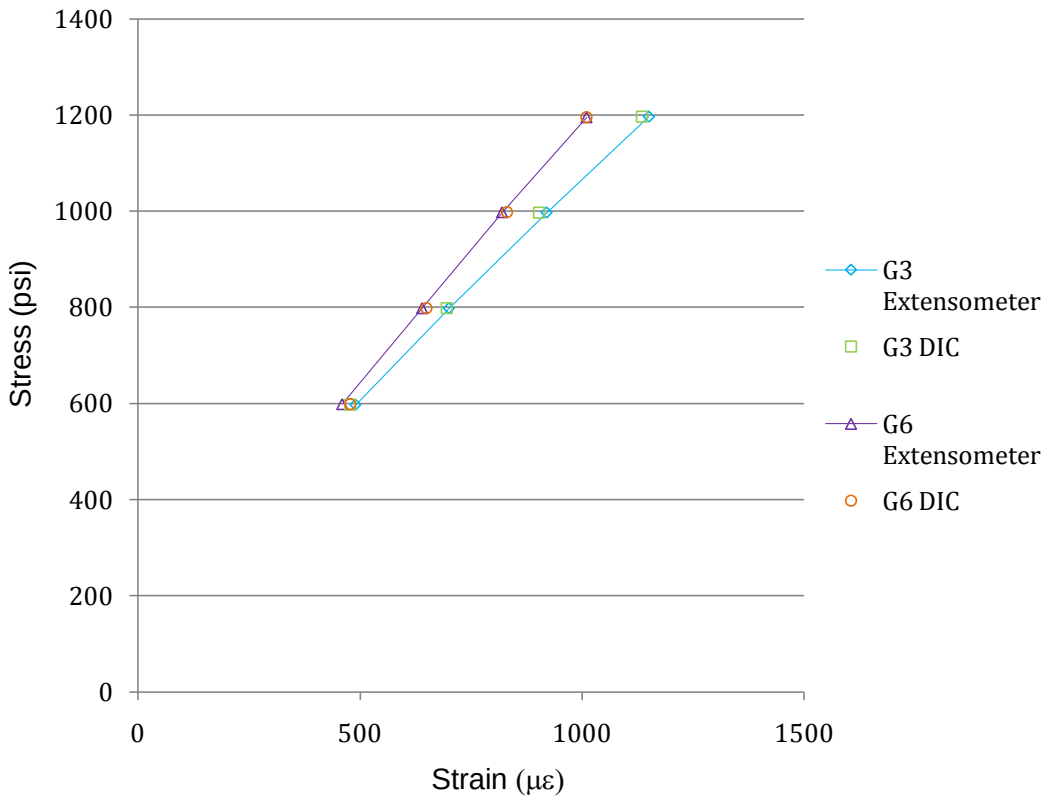

Figure 4.5 Room Temperature Stress-Strain Curve

Table 4.3 summarizes the modulus calculated from the slope of the linear portion of the stress-strain curve.

Table 4.3 Tensile Moduli based on Extensometer and DIC Strain Measurements

Specimen	Extensometer Modulus (Msi) [GPa]	DIC Modulus (Msi) [GPa]	Percent Error (%)
G3	0.91 [6.27]	0.92 [6.34]	0.97%
G6	1.09 [7.52]	1.12 [7.72]	2.98%

The moduli calculated independently from extensometer readings and DIC data agree within 3% illustrating the ability of non-contact DIC to generate accurate measurements of

material properties. Consistent agreement is seen between extensometer and DIC results. Figure 4.6 shows a comparison of normalized moduli between 8 tensile tests and Figure 4.7 shows the error in this data set to be within 2%.

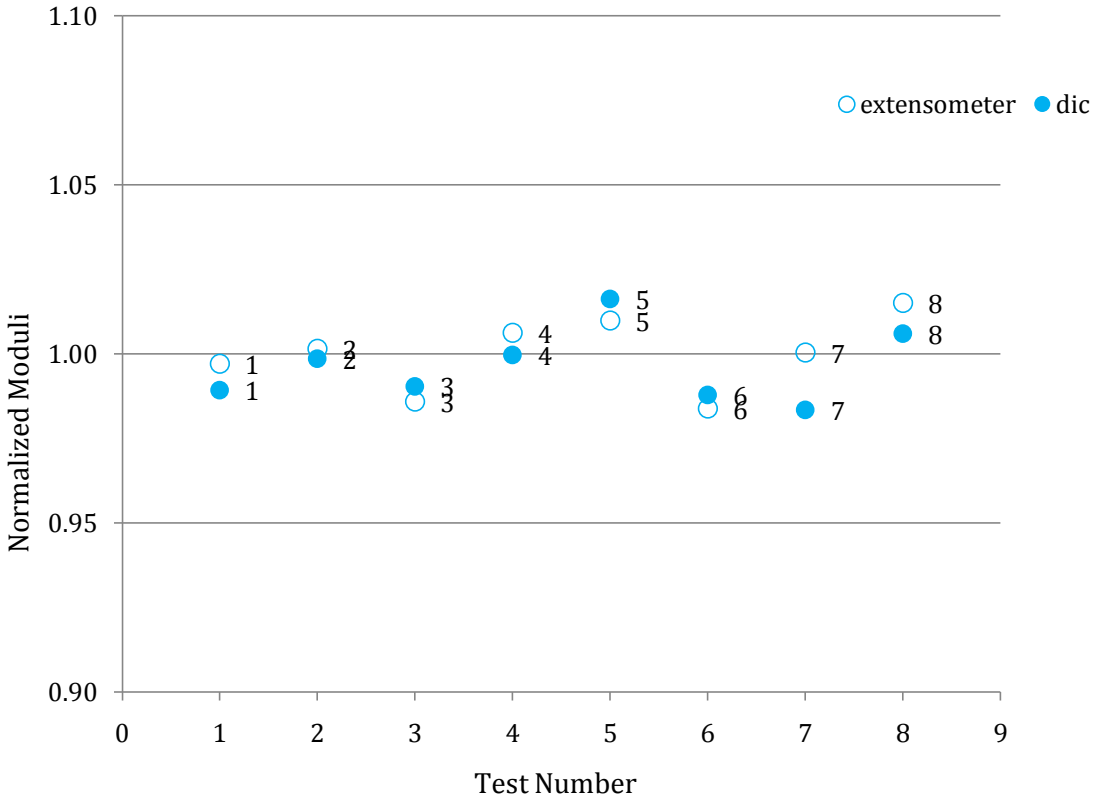

Figure 4.6 Comparison of Longitudinal Moduli Calculated by Extensometer and DIC Strain Measurements

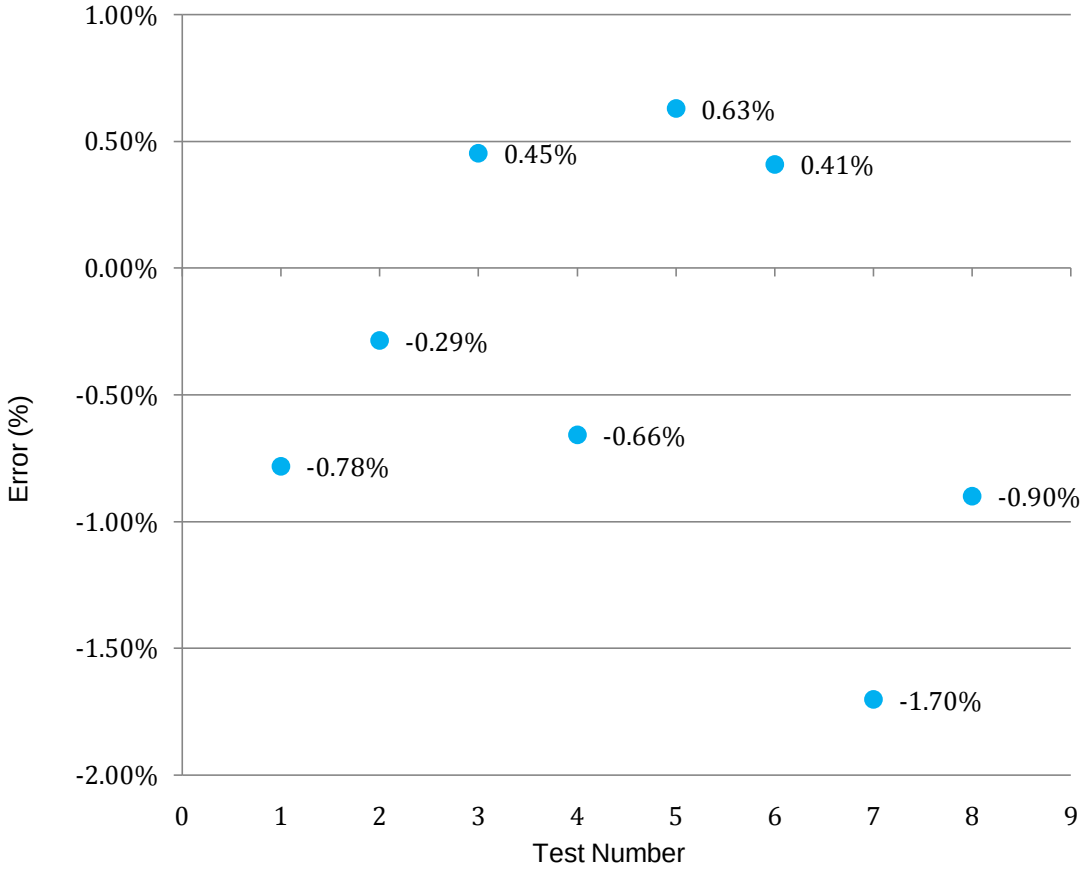

Figure 4.7 Error in Moduli Calculated by Extensometer and DIC Strain Measurements

A comparison of the longitudinal elongation and transverse contraction, shown in Figure 4.8, yields a measurement of Poisson's ratio for graphite of 0.12 and 0.09 for two tests.

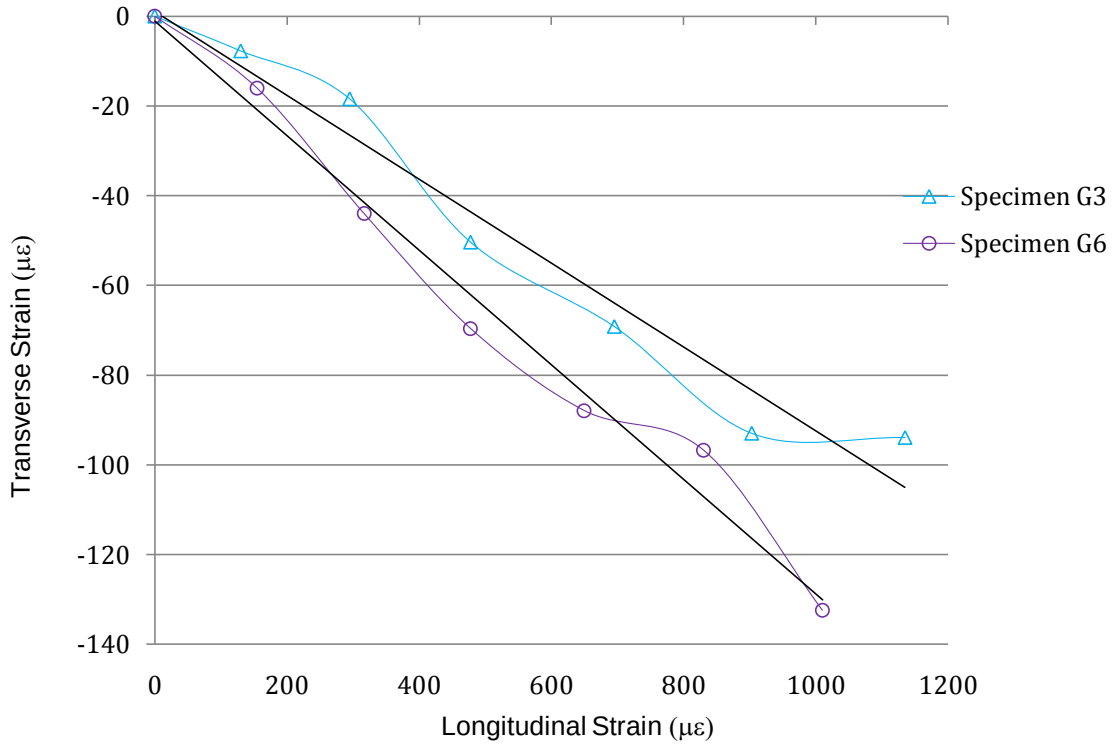

Figure 4.8 Comparisons of Room Temperature Transverse and Longitudinal Strains

The brittle nature of the graphite specimens makes it harder to resolve transverse strains because the displacement is on the order of 0.5 pixels for an axial load of 120 lbs (534 N). Measurements taken from material systems that exhibit a more pronounced contraction due to Poisson's effect would likely be more linear.

The full-field strain plots for the transverse and longitudinal directions (Figs. 4.9 - 4.10) show the homogeneity of the displacement and strain fields for room temperature graphite tests.

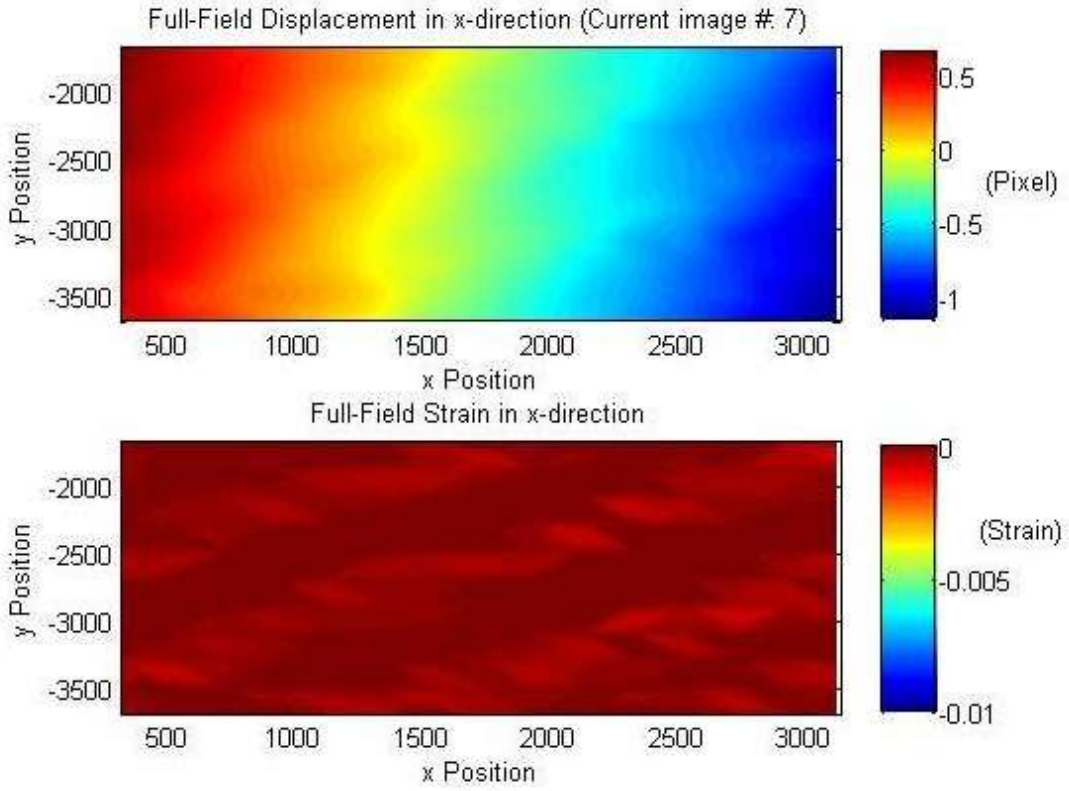

Figure 4.9 Full-field Transverse Strain at Room Temperature

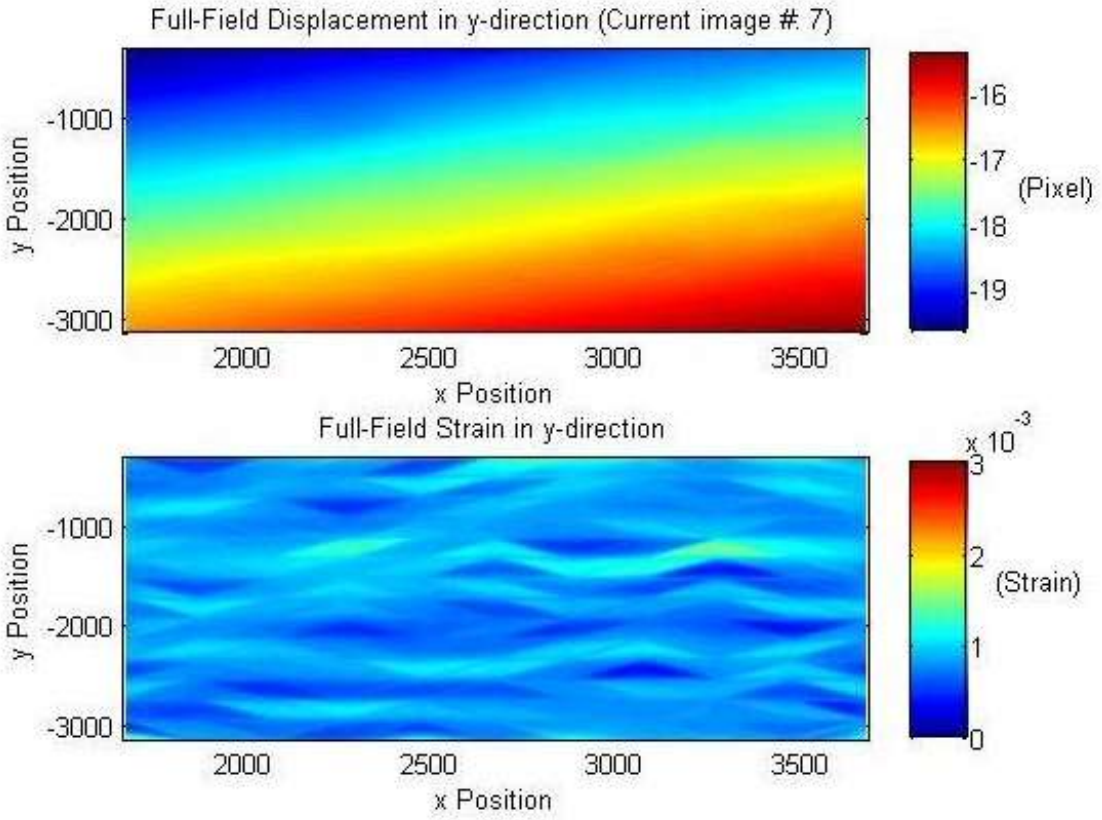

Figure 4.10 Full-field Longitudinal Strain at Room Temperature

The good correlation between independent strain measurement techniques confirms the capabilities of digital image correlation and provides the confidence needed to extend the application to high-temperature cases where the ability to measure data for direct comparison does not exist.

4.2 Ultra-High Temperature Tensile Tests using DIC

The nature of the test specimens presents a large challenge for high temperature testing. Graphite is a very brittle material sensitive to compressive loading and out-of-plane bending loads. In order to not crush the grip area of the specimens, tightening of the gripping

bolts was limited to a torque of 15 in-lb (1.69 N-m); slip in the grip area was observed in several tests.

Applying a pre-load to the specimen to compensate for thermal expansion prior to heating to 2000°F (1093˚C) was difficult due to the brittle nature of the specimen. Failure at high temperature primarily occurred at low load levels, limiting the number of data points collected. In order to reach higher loading, the use of a different material system is required.

Significant optical distortion was noted in high temperature images that caused significant de-correlation in several tests. This could be caused by (1) quality of viewing glass plane, and (2) distortion due to heated gas in the optical plane [9-13].

A basic pane of window glass was used in this work and literature suggests that optical quality glass should be used when viewing the specimen to reduce distortion [9-13]. Furthermore, large cracks form in the glass pane due to an significant temperature difference between heated gas in the enclosure box and ambient air outside. The use of quartz glass (high-temperature resistant) or an un-mounted hot mirror (high optical quality) or combinations of both are possible solutions to reduce distortion. To resolve the issue completely, the set-up could be modified so that the end of the telecentric lens is inside the enclosure box, negating the need for any viewing glass.

It is suggested in several research investigations that the effect of refractive index variations in heated gas in-line with the optical plane can cause severe distortion [9-13]. In the set-up used herein, heated gas from the insulating enclosure surrounding the specimen may escape through the imaging window, passing directly in front of the camera. The addition of a small fan to disperse the heated gas was implemented by Lyons *et al* [9] perpendicular to the specimen, which alleviated the source of optical distortion.

The strain per image measured for four material specimens tested at 2000°F (1093˚C) are presented. As shown in Figure 4.11, significant variations in strain measurements exist due to the optical distortion present in the images.

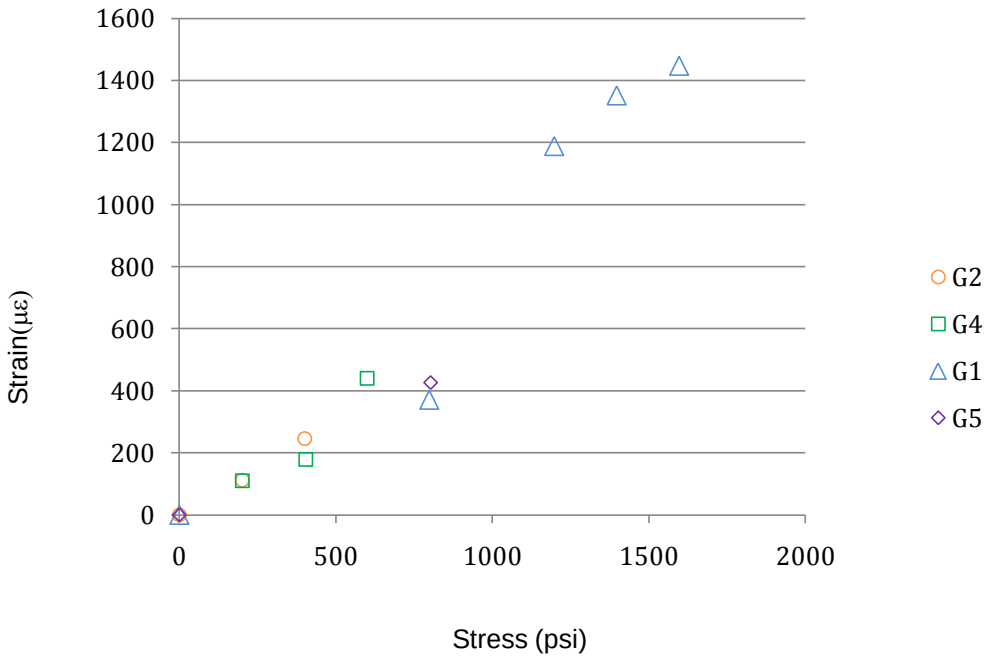

Figure 4.11 Longitudinal Strain per Stress Level for High Temperature Tensile Tests

As shown in room temperature tests, measurements are less accurate at low strain levels and these data points are generally disregarded from subsequent calculations. However, in the case of high temperature tests, the only data points able to be obtained to date are at low strain levels because of premature failure. The data shown herein demonstrates the potential for high accuracy strain measurement at high temperatures.

Outlying strain measurements are disregarded when generating stress-strain diagrams as shown in Figure 4.12.

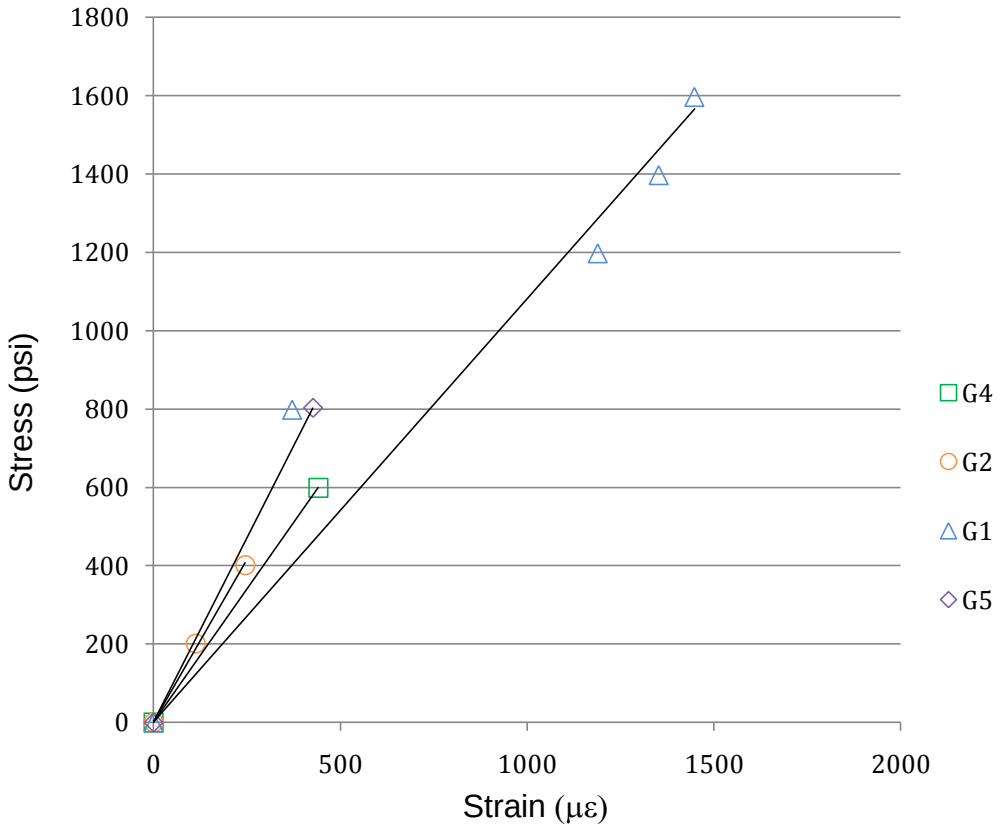

Figure 4.12 Ultra-High Temperature Stress-Strain Curve

Moduli are measured from the slope of the linear region of the stress-strain curve and presented in Table 4.4.

Table 4.4 Calculated Moduli for High Temperature Tensile Tests

	G1	G2	G4	G5
Modulus (Msi)	1.08	1.66	1.36	1.88

Measurements of transverse strain at high temperature were not accurate due to the low strain/load levels beyond the resolution capabilities of DIC at low strain levels, even with sub-pixel resolution. Subsequent testing on an alternate less brittle material system capable of withstanding higher loads would provide means to obtain transverse strain measurements.

Full-field strain plots at ultra-high temperature illustrate the effects of optical distortion on strain measurements (Figs. 4.13 and 4.14)

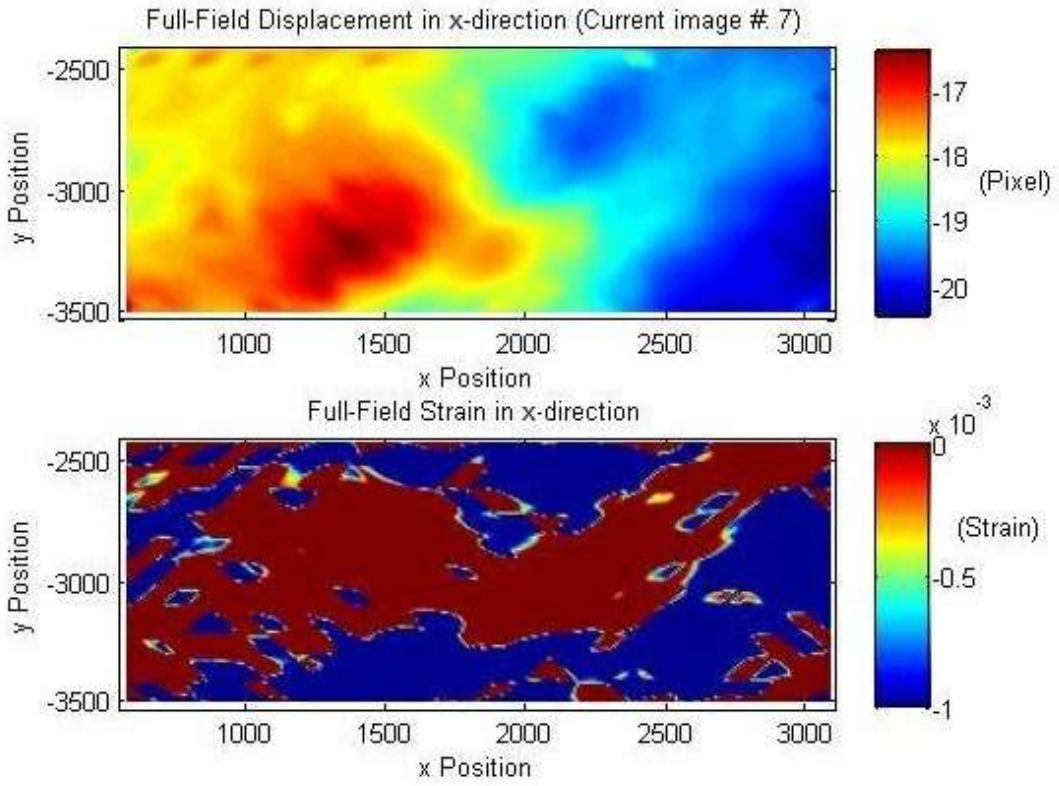

Figure 4.13 Full-field Transverse Strain at 2000˚F (1093˚C)

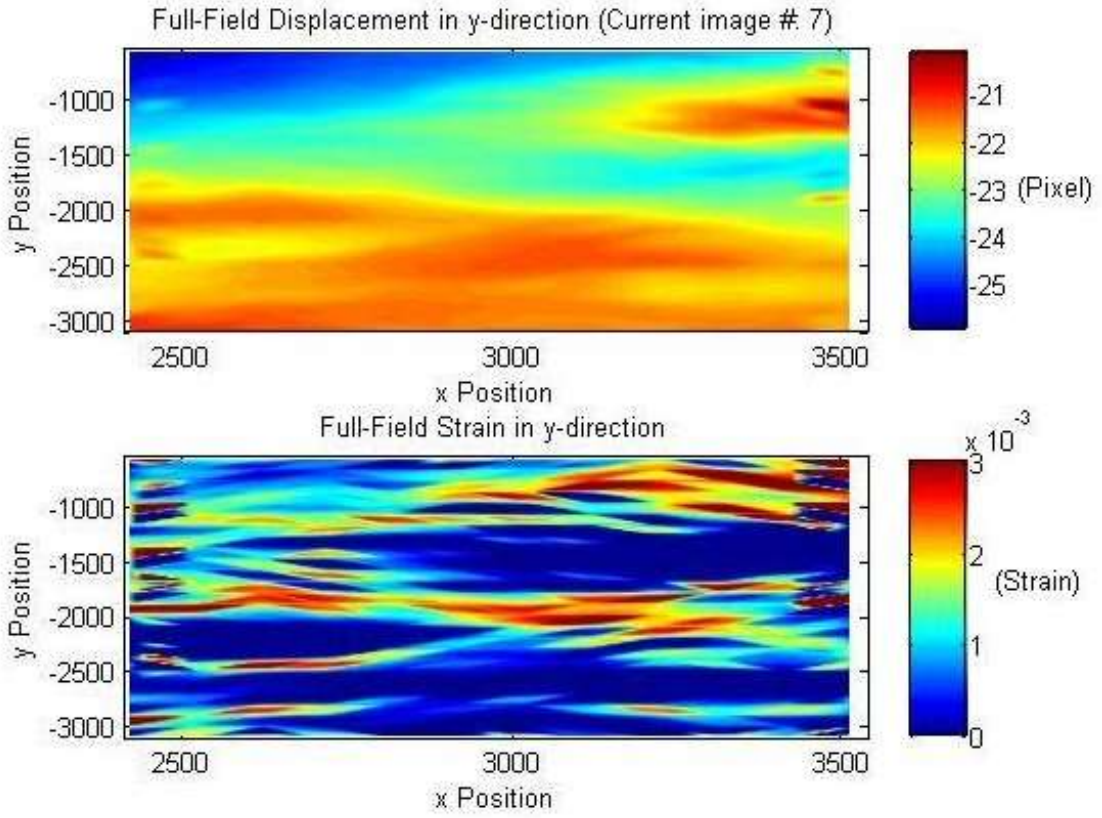

Figure 4.14 Full-field Longitudinal Strain at 2000˚F (1093˚C)

CHAPTER 5

CONCLUSIONS AND RECOMMENDATIONS

Significant progress has been made toward the development of ultra-high temperature thermo-mechanical material characterization capabilities using digital image correlation. The ability to perform a tensile test on material specimens heated to 2000°F (1093˚C) has been achieved through the design of a combined temperature control and high-temperature gripping mechanism. Heating capabilities and temperature sensing have been verified up to 3000°F (1649˚C).

It is shown that accurate measurements of strain can be obtained through the use of digital image correlation Matlab [7] based software [8] using a high-quality imaging system insensitive to optical effects caused by out-of-plane displacement. Comparison of DIC results with independent measurements taken with an extensometer show agreement within 2% for strain readings and 2% for calculated modulus. Measurements of transverse strain and Poisson's ratio can also be obtained using this method. A viable ultra-high temperature resistant tracking pattern is achieved using a sodium-silicate based adhesive.

The DIC method is shown to be less accurate at low strain levels, and is therefore not recommended for measurement of very small strains. Good data correlation is seen for measurements performed on material specimens that can achieve high load/strain levels.

Results from ultra-high temperature tests show the potential to obtain high-contrasting images free from radiated light at a constant temperature of 2000°F (1093˚C) and the ability to track displacements within these images. De-correlation effects are seen within the images and

are thought to be the result of optical distortion due to low quality viewing glass and heated gas in the optical path. Potential is seen to obtain strain measurements at ultra-high temperature for material characterization but further tests must be performed to confirm this postulation. Sources of optical distortion must be isolated to determine their contributing effect to further refine the design of the imaging system.

The use of fused quartz glass and hot mirror are recommended to replace the viewing glass in the enclosure box to reduce the effects of refractive index variations within the glass on captured images. Placing the end of the telecentric lens inside the enclosure box would negate the need for a viewing glass altogether. Methods of reducing stagnant heated gas in the optical path, such as fans to circulate the flow, must be tested to determine the best way to alleviate this issue. The experimental set-up can be modified to perform testing in a vacuum chamber eliminating the need for the inert atmosphere and thus, removing heated gas altogether from the optical plane.

Ultra-high temperature testing at typical re-entry temperatures of 3000°F (1649˚C) will require further refinement of the experimental set-up. Sizeable burn-off of the surface pattern generated using the sodium-silicate adhesive is observed to begin at 2800°F (1538˚C) and continues throughout the test duration. Images with contrasting patterns can be captured, however, significant de-correlation is observed due to the disappearance of features between images. Alternative application techniques, ceramic adhesives and refractory paints are being investigated to determine the best approach to create a lasting surface pattern.

Currently capabilities of the lighting and filter system allow us to capture images at 2000°F (1093˚C) solely in the blue channel by using a narrow blue band-pass filter to remove the effect of radiated light and providing additional blue light illumination to the specimen surface. The intensity of radiated light is a function of surface temperature at a given wavelength, therefore, at 3000°F (1649˚C), the energy of the radiated light in each peak wavelength will shift requiring the filter system to be adjusted accordingly.

A newly acquired Northstar Computed Tomography (CT) Scan machine provides the opportunity to extend the body of work to examine specimens before and after testing using high-resolution non-destructive volumetric imaging. Research should be conducted as to achieving a load/temperature control system to work in conjunction with the CT Scan machine to leverage the opportunity to use cutting-edge 3-D volumetric correlation to measure strain throughout a volume to understand the internal behavior of the material system that is not measurable using 2-D surface-strain measurement.

REFERENCES

[1] Glass, D.E., “Ceramic Matrix Composite (CMC) Thermal Protection Systems (TPS) and Hot Structures for Hypersonic Vehicles,” *Proceedings of the 15th AIAA Space Planes and Hypersonic Systems and Technologies Conference*, Dayton, OH, Apr 28-1, 2008.

[2] Beckwith, T.G., Marangoni, R.D., and Leinhard V, J.H., Mechanical Measurements 6th Edition, Pearson, 2007, Chap 12.

[3] Sutton, M.A., Orteu, J.J., Schreiner, H.W., Image Correlation for Shape, Motion and Deformation Measurements, Springer, New York, 2009, Ch. 1-6.

[4] Pan, B., Qian, K., Xie, H., and Asundi, A., “Two-Dimensional Digital Image Correlation for In-Plane Displacement and Strain Measurement: A Review,” *Measurement Science and Technology*, Vol. 20, No. 6, 2009, pp. 1-17.

[5] Thompson, R.J., and Hemker, K. J., “Thermal Expansion Measurements on Coating Materials by Digital Image Correlation,” *Proceedings of the SEM Annual Conference and Exposition on Experimental and Applied Mechanics*, Springfield, MA, June 4-6, 2007, pp. 1058-1067.

[6] Sutton, M.A., et al., “The Effect of Out-of Plane Motion on 2D and 3D Digital Image Correlation Measurements,” *Optics and Lasers in Engineering*, Vol., 46, No. 10, 2008, pp. 746-757

[7] Matlab, Ver. 7.11.0.584 (R2011b), Mathworks, Inc. Natick, MA, 2011.

[8] Eberl, C., Thompson R., Gianola, D., Sharpe Jr, W., and Hemker, K., “Digital Image Correlation and Tracking with Matlab”, http://www.mathworks.com/matlabcentral/fileexchange, 2006.

[9] Lyons, J.S., Liu, J., and Sutton, M.A., “High Temperature Deformation Measurements Using Digital-Image Correlation,” *Experimental Mechanics*, Vol. 36, No. 1, 1996, pp. 64-70.

[10] Völkl, R., and Fischer, B., “Mechanical Testing of Ultra-High Temperature Alloys,” *Experimental Mechanics*, Vol. 44, No. 2, 2004, pp. 121-127.

[11] Pan, B., Wu, D., and Xia, Y., “High-Temperature Deformation Field Measurement by Combining Transient Aerodynamic Heating Simulation System and Realiability-Guided Digital Image Correlation,” *Optics and Lasers in Engineering*, Vol. 48, No. 9, 2010, pp. 841-848.

[12] Grant, B.M.B., Stone, H.J., Withers, P.J., and Preuss, M., “High-Temperature Strain Field Measurement Using Digital Image Correlation,” *The Journal of Strain Analysis for Engineering Design*, Vol. 44, No. 4, 2009, pp. 263-271.

[13] Pan, B., Wu, D., Wang, Z., and Xia, Y., “High-Temperature Digital Image Correlation Method for Full-Field Deformation Measurement at 1200˚C,” *Measurement Science and Technology*, Vol. 22, No. 1, 2011.

[14] VIC-2D, 2009, Correlated Solutions, Columbia, SC, 2009.

[15] StrainMaster 2D/3D DIC, LaVision, Inc, Ypsilanti, MI, 1989-2011.

[16] Mathematica, Ver. 8.0.0.1, Wolfram Research Inc., Champaign, IL, 1988-2010.

[17] Multi-Comm, Ver. 3.16, Athena Controls, Inc., Leominster, MA. 2002.

[18] Bacos, M.P., “Carbon-Carbon Composites: Oxidation Behavior and Coatings protection,” *Journal de Physique III*, Vol. 3, Nov. 1993, pp. 1895-1903.

[19] Bluehill 2 Materials Testing Software, Illinois Tool Works, Inc., Norwood, MA.

[20] Petrozzo, R.A., and Singer, S.W., “Telecentric Lenses Simplify Non Contact Metrology,” *Test & Measurement World*, 2001, pp. 4-9.

[21] Canon EOS Utility, Canon U.S.A. Inc, Lake Success, NY.

BIOGRAPHICAL INFORMATION

Julia was born in Edmonton, Alberta, Canada on October 30, 1986. She graduated with honors from Harry Ainlay Composite High School in 2004 with International Baccalaureate certificates in History, French and Mathematics. She received the Alexander Rutherford Scholarship and the University of Alberta Academic Excellence Scholarship for her achievements.

Julia began her undergraduate career at the University of Alberta in the fall of 2004. She graduated with a Bachelor's of Science degree specializing in Astrophysics in 2008. After graduation, she moved to Texas to pursue a graduate degree in Aerospace Engineering at the University of Texas at Arlington. She began working with Dr. D. Stefan Dancila in September 2009. After completion of her Master of Science degree, Julia plans to continue her education in pursuit of a PhD at UT Arlington.

She is a member of the National Scholar's Honor Society, Golden Key International Honors Society and Kappa Alpha Theta Women's Fraternity.